A cytomegalovirus immunevasin triggers integrated stress response-dependent reorganization of the endoplasmic reticulum.

Running Title: HCMV UL148 reorganizes the ER.

Hongbo Zhang[a,1], Clarissa Read[d,e,1], Christopher C. Nguyen[a,1], Mohammed N.A. Siddiquey[a], Chaowei Shang[c], Cameron M. Hall[a], Jens von Einem[d], and Jeremy P. Kamil[a,b #]

[a]Department of Microbiology and Immunology,

[b]Center for Molecular and Tumor Virology

[c]Research Core Facility

LSU Health Sciences Center, Shreveport, Louisiana, USA

[d] Institute of Virology, Ulm University Medical Center,

[e]Central Facility for Electron Microscopy, Ulm University

Ulm, Germany

[1] these authors contributed equally to the study

Running Head: HCMV UL148 Remodels the ER

#Address correspondence to Jeremy P. Kamil, jkamil@lsuhsc.edu

ABSTRACT. Human cytomegalovirus (HCMV) encodes an ER-resident glycoprotein, UL148, which activates the unfolded protein response (UPR) but is fully dispensable for viral replication in cultured cells. Hence, its previously ascribed roles in immune evasion and modulation of viral cell tropism are hypothesized to cause ER stress. Here, we show that UL148 is necessary and sufficient to drive the formation of large ER-derived structures that occupy up to 7% of the infected cell cytosol. The structures are found to be sites where UL148 coalesces together with cellular proteins involved in ER quality control, such as Hrd1 and EDEM1. Ultrastructural analyses of the structures reveal tortuous, densely packed segments of collapsed ER which connect to distended cisternae. Notably, UL148 accumulates in a detergent-insoluble form during infection while a homologous rhesus cytomegalovirus immunevasin that fails to cause ER reorganization remains soluble. During induced ectopic expression of a UL148-GFP fusion protein, punctate signals traffic to accumulate at prominent structures that exhibit poor recovery of fluorescence after photobleaching. Small molecule blockade of the integrated stress response (ISR) prevents the formation of puncta, leading to a uniform reticular fluorescent signal. Accordingly, ISR inhibition during HCMV infection abolishes the coalescence of UL148 and Hrd1 into discrete structures. Given that UL148 stabilizes immature forms of a receptor binding subunit for a viral envelope glycoprotein complex of pivotal importance for HCMV infectivity, which is otherwise particularly susceptible to ER associated degradation, our results imply that stress-dependent ER remodeling contributes to viral cell tropism.

48 **IMPORTANCE.**

49 Perturbations to ER morphology occur during infection with various intracellular
50 pathogens and in certain genetic disorders. We identify that an HCMV gene product,
51 UL148, profoundly reorganizes the ER during infection, and is sufficient to do so when
52 expressed on its own. Our results reveal that UL148-dependent reorganization of the
53 ER is a prominent feature of HCMV infected cells. Moreover, we find that this example
54 of virally induced organelle remodeling requires the integrated stress response (ISR), a
55 stress adaptation pathway that contributes to a number of disease states. Since ER
56 reorganization accompanies the roles of UL148 in HCMV cell tropism and intracellular
57 retention of the immune cell co-stimulatory ligand CD58, our results may have
58 implications for understanding the mechanisms involved. Furthermore, our findings
59 provide a basis to utilize UL148 as a tool to investigate organelle responses to stress
60 and to identify novel drugs targeting the ISR.

61 **INTRODUCTION.**

62 UL148 is a human cytomegalovirus (HCMV) ER-resident glycoprotein that plays
63 roles in evasion of cell-mediated immunity and shows intriguing effects on cell tropism.
64 During infection of epithelial cells, viruses disrupted for *UL148* replicate to produce
65 roughly 100-fold enhanced levels of infectious progeny virions compared to wildtype (1).
66 These effects correlate with reduced expression of glycoprotein O (gO), a subunit of a
67 heterotrimeric viral glycoprotein H (gH) / glycoprotein L (gL) complex (gH/gL/gO) on the
68 virion envelope that is required for the infectivity of cell-free virions (2-4), and which
69 endows the virus with the capacity to utilize the platelet derived growth factor receptor α
70 (PDGFRα) as an entry receptor (5-7). Accordingly, UL148 has been found to stabilize
71 immature forms of gO prior their assembly into gH/gL/gO heterotrimers (1, 8). Despite
72 that UL148 does not stably associate with gO, the data suggest that it may interact with
73 gH (1).

74 UL148 also physically associates with CD58 (LFA-3), a co-stimulatory ligand for
75 natural killer cells and T-lymphocytes, preventing its presentation at cell surface (9).
76 Although the mechanisms by which UL148 stabilizes gO and retains CD58 within the
77 ER remain unknown, UL148 strongly contributes to activation of the unfolded protein
78 response (UPR) during infection, and is sufficient to activate the UPR when ectopically
79 expressed in non-infected cells (10). UL148 co-purifies from infected cells with SEL1L,
80 an adaptor subunit of ER-based E3 ubiquitin ligase Hrd1 that plays important roles in
81 ER-associated degradation (ERAD) of terminally misfolded glycoproteins (8). This
82 suggests a physical interaction with ERAD machinery, which may be germane to the
83 mechanism by which UL148 activates the UPR.

84 Here, we show that expression of UL148 is necessary and sufficient to induce
85 unusual ER structures at which large quantities of ER factors involved in glycoprotein
86 quality control accumulate. In electron microscopy analyses, we find that the UL148
87 induced ER-structures are comprised of densely packed, tortuous ER membranes that
88 form connections with tubules of highly distended cisternal space. Our results may
89 have implications for understanding the mechanisms by which UL148 regulates viral cell
90 tropism and contributes to viral evasion of cell-mediated immunity. Further, our findings
91 suggest that ER remodeling events triggered by UL148 are indicative of an adaptive
92 response of eukaryotic cells to proteotoxic stress involving the secretory pathway.
93

94 **RESULTS.**

95

96 **UL148 causes reorganization of ER quality control proteins into unusual globular**
97 **structures.**

98 The HCMV ER-resident glycoprotein UL148 was previously observed to co-
99 localize with the ER marker calnexin during infection (1). Nonetheless, calnexin staining
100 did not show the uniform reticular pattern characteristic for the ER marker. We later
101 noticed that cells infected with a *UL148*-null virus showed uniform calnexin staining (see
102 below). To formally determine whether UL148 influences calnexin localization, we
103 compared fibroblasts at four days post-infection with either wildtype (TB_WT) or *UL148*-
104 null mutant (TB_148_{STOP}) viruses derived from an infectious bacterial artificial
105 chromosome (BAC) clone of HCMV strain TB40/E (**FIG 1**). In cells infected with
106 wildtype virus, calnexin antibodies stained unusual globular structures at the cell
107 periphery, as expected (1) (**FIG 1A, 1C, SI FIG S1A**). However, in cells infected with
108 the *UL148*-null virus, calnexin staining was uniform throughout the cytosol (**FIG 1B-C**),
109 as would be expected for an ER marker in uninfected cells. The staining pattern for
110 Hrd1, another ER marker, likewise indicated accumulation at unusual globular
111 structures during wildtype HCMV infection, but not during infection with *UL148*-null
112 mutant viruses (**FIG 1, SI FIG S1A**). Because calnexin and Hrd1 staining showed
113 uniform distribution in *UL148*-null virus infected cells, and because *UL148* is fully
114 dispensable for efficient viral replication in fibroblasts (1), these results suggest that
115 redistribution of these ER markers depends on UL148.

116 As expected (11, 12), antibodies specific for the HCMV envelope glycoprotein,
117 glycoprotein H (gH), stained a juxtanuclear compartment, termed the cytoplasmic virion
118 assembly compartment (cVAC), which does not involve the ER (**FIG 1**). Similarly
119 contrasting staining patterns for Hrd1 and/or calnexin were observed in cells infected
120 with wildtype versus *UL148*-null mutants of clinical HCMV strains Merlin and TR (**FIG**
121 **S1**). Reciprocally, we restored a functional *UL148* at its native locus in the context of a
122 BAC clone of HCMV strain AD169, which spontaneously lost most of the gene in the
123 course of extensive genetic rearrangements and deletions that accumulated during
124 serial passage in tissue culture. In cells infected with AD169 repaired for UL148, but
125 not the *UL148*-null parental virus, the Hrd1 staining pattern showed obvious aggregation
126 into globular structures (FIG S1).
127 As similar differences in Hrd1 staining are observed between wildtype and
128 *UL148*-null infections of THP-1 macrophages, ARPE-19 epithelial cells and fibroblasts
129 (**FIG 1, FIG S1**), UL148-dependent reorganization of ER markers occurs in multiple cell
130 types. The calnexin staining pattern seen with four different primary clinical isolates
131 from patient throat swabs likewise indicated punctate globular structures. These
132 observations, taken together with the results from formal comparisons of wildtype
133 versus *UL148*-null mutants of four different BAC-cloned HCMV strains (**FIG 1, FIG S1**),
134 argue that UL148 profoundly affects the ER during natural infection.
135 We measured the three-dimensional volume of UL148-dependent Hrd1
136 structures from sixteen cells fixed at 96 hpi with strain TB40/E. On average, the
137 structures occupied 303.3 μm^3 (SEM: +/- 24.8) out of a total cell volume of 7657 μm^3
138 (SEM:+/- 651.0), as measured using a phalloidin-fluorophore conjugate to detect the

139 actin cytoskeleton (**FIG 1D-E**). Subtracting the volume of nuclei, as indicated by 4′,6-
140 diamidino-2-phenylindole [DAPI] (average nucleus: 1360 μm^3, SEM:+/-129.4), we
141 calculate that, on average, the structures occupy 5.2% of the cytosolic volume (SEM: +/-
142 0.61%, range: 2.0% – 7.0%). Based on these findings, taken together with results
143 comparing additional WT versus *UL148*-null mutant HCMV strains (**FIG S1**), we
144 conclude that the UL148-dependent ER structures are a prominent feature of HCMV-
145 infected cells.

146 UL148 substantially contributes to activation of the unfolded protein response
147 (UPR) during HCMV infection (10), and co-purifies from infected cells with SEL1L (8),
148 an adaptor subunit for the E3 ubiquitin ligase Hrd1, which plays crucial roles in ER-
149 associated degradation (ERAD) of terminally misfolded glycoprotein substrates (13).
150 Hence, the accumulation of Hrd1 and calnexin at unusual structures during wildtype but
151 not *UL148*-null infection may suggest that structures form in response to defects in ER
152 quality control (ERQC) caused by UL148. Under conditions of proteasome inhibition,
153 overexpression of certain misfolded glycoproteins causes cellular factors involved in
154 ERQC, such as calnexin, to compartmentalize from the rest of the ER, while other ER
155 markers such as BiP (Grp78) or protein disulfide isomerase (PDI) remain largely
156 unaltered (14-16).

157 To gain further insights into the nature of these peculiar ER structures, we set out
158 to develop a more comprehensive understanding of their protein composition by
159 comparing the localization of selected ER markers in cells fixed at 96 h post-infection
160 (hpi) either with TB_148^{HA} (1), a derivative of HCMV strain TB40/E that expresses at the
161 C-terminus of UL148 the nonapeptide epitope YPYDVPDYA from influenza A

162 hemagglutinin (HA), or with TB_159^{HA}, an isogenic control virus in which we replaced
163 the *UL148* coding sequence with the UL148 homolog from rhesus cytomegalovirus,
164 Rh159, likewise fused at its C-terminus to an HA-tag. We considered the TB_159^{HA}
165 virus to be an appropriate control for the following reasons. Firstly, Rh159 and UL148
166 exhibit ~30% identity at the amino acid level and both glycoproteins localize to the ER
167 and block cell surface presentation immune cell activating ligands; UL148 retains CD58,
168 a ligand for CD2, while Rh159 retains NKG2D ligands of the MIC- and ULBP families (1,
169 9, 17). Secondly, Rh159 is expressed from TB_159^{HA} at comparable levels and with
170 similar kinetics observed for UL148 from TB_148^{HA}, and the two viruses replicate
171 indistinguishably in fibroblasts (**FIG 2**). Moreover, Rh159 does not appear to activate
172 the UPR (10), and ERQC markers fail to coalesce into unusual structures during
173 infection with TB_159^{HA} (**FIG 3**). Notably, ER structures likewise fail to occur in rhesus
174 fibroblasts during infection with a recombinant rhesus cytomegalovirus (RhCMV)
175 engineered to express an HA-tag fused at the C-terminus of Rh159 (**FIG S1**). This
176 argues against the possibility that Rh159 requires the context of rhesus cells to
177 redistribute ER markers in a manner analogous to what is seen for UL148 during HCMV
178 infection, and instead suggests that UL148 and Rh159 authentically differ in their effects
179 on the secretory pathway.

180 In cells infected with TB_148^{HA}, HA antibody staining indicated localization of
181 UL148 to globular structures, as expected (1). Antibody signals during indirect confocal
182 immunofluorescence detection of cellular ER resident proteins involved in ERQC,
183 including calnexin, Hrd1, SEL1L, Herp, valosin containing protein (VCP, p97), and
184 EDEM1, co-localized to a strong degree with signals from HA-tagged UL148 (**FIG 3-4**).

185 These results indicate that a number of ERQC factors coalesce with UL148 to form
186 prominent globular structures in infected cells. In contrast, uniform ER staining patterns
187 were observed with antibodies specific for PDI and calreticulin (CALR), indicating that
188 these ER markers do not localize to the UL148 structures (**FIGS 3Q, 3S**). Intriguingly,
189 antibody signals detecting reticulon 3 and ribophorin 1, which are markers for smooth
190 ER and rough ER, respectively, each appreciably co-localized with UL148 (HA) signal at
191 the induced structures (**FIGS 3K, 3M)**, which indicates that the structures may involve
192 both rough and smooth ER. LC3B failed to co-localize with the structures (**FIG S2**), as
193 would be expected given that the virus inhibits macroautophagy at late times during
194 infection (18, 19). Nevertheless, we obtained evidence suggesting the induced
195 structures are enriched for a related mammalian ATG8 ortholog, GABARAP (**FIG 3O**).
196 In cells infected with TB_159^{HA}, all of the ER markers we examined showed
197 uniform, reticular staining, as did the anti-HA signal detecting Rh159 (**FIG 3B, D, F, H,**
198 **J, L, N, P, R, T**). EDEM1, in addition to showing reticular staining, also labeled puncta
199 associated with the nucleus (**FIG 3J**), which may represent enriched levels of the
200 protein at the rough ER membranes associated with the nuclear envelope, although we
201 cannot exclude the possibility of spurious intranuclear staining. Nonetheless, the
202 punctate nuclear signal for EDEM1 was much less pronounced in the TB_148^{HA}
203 infected cells (**FIG 3I**). GABARAP antibodies stained the cVAC in TB_159^{HA} infected
204 cells, but also showed a much weaker reticular signal that may indicate ER staining.
205 Even though we took steps to block viral Fc receptors, which can cause rabbit
206 antibodies to non-specifically label the cVAC (20), it is plausible that GABARAP
207 antibody signal from the cVAC reflects incomplete blocking of viral Fc receptors. For

208 both viruses, antibodies specific for syntaxin-6 (STX6) and gH, as expected, stained the
209 juxtanuclear cVAC structure (11, 12, 21), which was previously found to be altogether
210 distinct from the UL148 staining pattern (1) (**FIG S2**).

211 To quantify the degree of co-localization with UL148, we calculated Pearson's
212 correlation coefficients from a minimum of thirty TB_148^{HA} infected cells per staining
213 condition, comparing the signal overlap for each ER marker to the HA signal from
214 UL148. The correlation coefficients (*r*) for EDEM1, Hrd1, reticulon-3 (RTN3), SEL1L
215 and calnexin ranged from 0.8 to 0.72, which suggests that these proteins extensively
216 co-localize with UL148 at 4 days post-infection (dpi) (**FIG 4**). Meanwhile, GABARAP,
217 VCP, ribophorin-1 (RPN1), and Herp showed *r* values in the range of 0.54 to 0.51,
218 indicating a moderate degree of co-localization with UL148. However, the ER markers
219 CALR and PDI, and the TGN marker syntaxin-6, gave *r* values of close to zero, which
220 confirms that these markers either do not co-localize with UL148 or show only a
221 negligible degree of association with UL148 at the induced structures.

222 From these results, we conclude that the UL148-dependent ER structures are
223 enriched for cellular markers associated with glycoprotein quality control. In this regard,
224 the structures resemble the "ER quality control (ERQC) compartments" described by G.
225 Lederkremer and colleagues (14, 15, 22). We further conclude that Rh159 cannot
226 substitute for UL148 to redistribute ERQC markers.

227

228 **VCP and Hrd1 are recruited to incipient UL148 ER structures prior to calnexin.**

229 To determine whether there might be differences in the kinetics of recruitment of
230 ERQC markers during formation of the ER structures, we examined a series of time

231 points from one to four days post-infection (dpi) with wild-type HCMV carrying HA-
232 tagged UL148, staining for three different ERQC markers, calnexin, Hrd1, and VCP,
233 alongside UL148 (HA). At 1 dpi the signal from UL148 was only faintly detected, as
234 expected (1), while each of the ER markers was readily detected, providing a readout of
235 their staining patterns prior to being substantially perturbed by UL148 (**FIG 5**). At 2 dpi,
236 we detected robust anti-HA signal, indicating the presence of UL148. At this time point,
237 UL148 exhibited intense signal at small globular puncta, which we interpret to represent
238 incipient UL148 structures, as well as more diffuse staining of a reticular structure
239 consistent with ER. Calnexin did not appreciably co-localize with the UL148 puncta until
240 at least 3 dpi, and the structures were not readily visualized by calnexin staining until 4
241 dpi (**FIG 5A**). In contrast, signals from Hrd1 and VCP staining were sufficient to mark
242 the UL148 puncta by 2 dpi, which suggests that these markers co-localize with UL148
243 at earlier points during the genesis of the ER structures. Notably, the appearance of
244 Hrd1 at the structures prior to calnexin is consistent with our previous results showing
245 that UL148 co-purifies from infected cells with SEL1L, an adaptor subunit for Hrd1 (8).
246 These results imply that basal elements of the ERAD machinery, exemplified by Hrd1
247 and VCP, may be recruited to UL148-induced ER structures prior to calnexin.
248
249 **Visualization of UL148-induced ER structures by electron microscopy.**
250 To discern the ultrastructural appearance of the UL148 structures and to formally
251 ascertain their relationship to the ER, we carried out transmission electron microscopy
252 (TEM) imaging of wildtype (TB_WT) and *UL148*-null (TB_148$_{STOP}$) infected fibroblasts at
253 5 dpi. In high pressure frozen and freeze-substituted infected fibroblasts, cells with a

254 high density of viral nucleocapsids within the nucleus were selected for analysis, as this
255 feature indicates late time points during infection when UL148 is abundantly expressed.
256 The TEM results revealed prominent globular and oblong structures in the cytoplasm of
257 wildtype virus infected fibroblasts, but not *UL148*-null infected controls (**FIGS 6-7**). The
258 structures stand out for their high electron-density, which may reflect the abundance of
259 ERQC proteins together with UL148 in these structures. Under higher magnification,
260 these areas are characterized by accumulations of densely packed ruffled membranes
261 and membranous material, which appear to be collapsed ER. Further, these membrane
262 accumulations were associated with smooth and partially rough ER structures with
263 seemingly enlarged cisternal space. Further, tomographic reconstruction of scanning
264 transmission electron microscopy (STEM) data suggest that densely packed ER
265 cisternae within the structures are interconnected and continuous in three-dimensional
266 space (**FIG 8B-C, SI Movie S1**).
267
268 **UL148 accumulates in a detergent-insoluble form during infection.**
269 Disease-associated variants of certain cellular proteins, such as the A103E
270 mutant of the calcium channel Orai1, and the E342K "Z" variant of alpha-1 antitrypsin (Z
271 A1AT), localize to anomalous ER structures reminiscent of those we observe to depend
272 on UL148 (16, 23-26). A103E Orai1 and Z A1AT are found to accumulate in detergent-
273 insoluble forms within the ER or within ER membranes, respectively, which indicates
274 aggregation or polymerization of these proteins, and suggests a mechanism for the
275 formation of ER structures by the proteins (16, 23, 26, 27). We therefore set out to
276 determine whether differences in solubility might correlate with the differing potentials

277 UL148 and Rh159 to cause ER reorganization and to activate the UPR (10). To
278 address this question, we infected fibroblasts with TB_148^{HA} or TB_159^{HA} at MOI 1 and
279 at various times post-infection prepared cell lysates in radioimmunoprecipitation assay
280 (RIPA) buffer. After subjecting the lysates to high-speed centrifugation, we examined
281 the relative levels of UL148 and Rh159 in the detergent-soluble supernatant and
282 detergent-insoluble pellet fractions.
283 A substantial portion of UL148 was detected from the detergent-insoluble
284 fractions at all time points tested (**FIG 9**). Furthermore, the percentage of UL148
285 detected within the insoluble fraction increased over time. In contrast, Rh159 was found
286 only in the detergent-soluble fraction. From these results, we conclude that UL148
287 accumulates in a detergent insoluble form during infection, and that Rh159 does not do
288 so. Because the relative mobility of the anti-HA immunoreactive band detected in
289 soluble and insoluble fractions obtained from TB_148^{HA} infected cells showed a relative
290 mobility of ~35 kD, which is indicative of the mature, endoH-sensitive glycoprotein (1),
291 these findings suggest that UL148 may aggregate or polymerize within the ER.
292
293 **UL148 is sufficient to compartmentalize the ER.**
294 Our data thus far demonstrate that UL148 is necessary during infection to cause
295 redistribution of cellular ER markers for glycoprotein quality control processes, such that
296 substantial portion of the ERQC machinery appears to become sequestered away from
297 the rest of the organelle into novel membranous structures. Because a number of viral
298 proteins that remodel the ER during infection are sufficient to alter ER morphology when
299 ectopically expressed [e.g. (28),(29), reviewed in (30)], we wondered whether UL148

300 expression is sufficient to induce ER structures akin to those seen during HCMV
301 infection. Making use of existing “tet-on” ARPE-19 epithelial cells that inducibly express
302 of either UL148 or Rh159, each carrying a C-terminal HA-tag (31), we induced
303 transgene expression for 48 h and subsequently stained for various cellular markers for
304 the ER, for ERQC as well as for LC3B and GABARAP, which are ATG8 family proteins
305 that mark autophagosome membranes.

306 In cells expressing UL148 (i148^{HA}), we observed that calnexin, Hrd1, EDEM1,
307 and VCP co-localize with UL148 at prominent globular structures reminiscent of those
308 observed during infection (**FIG 10**). The respective rough and smooth ER markers
309 ribophorin 1 (RPN1) and reticulon 3 (RTN3), as well as the ATG8 proteins LC3B and
310 GABARAP likewise co-localized to the UL148-induced structures. However, PDI and
311 CALR each failed to substantially co-localize with UL148 at the structures (**FIG 10**), or at
312 best showed only limited co-localization, consistent with our results from infected cells
313 (**FIG 3-4**). Signals from antibodies specific for a KDEL motif important for ER retrieval
314 of luminal ER residents, such as BiP, likewise showed only limited co-localization with
315 UL148. These results suggest that large portions of the ER are not involved in the
316 UL148 structures.

317 In cells expressing the UL148 homolog Rh159 (i159^{HA}), we detected uniform
318 cytoplasmic distribution of ER markers, as well as of HA-tagged Rh159, similar to what
319 we observed during infection with the recombinant HCMV TB_159^{HA} (**FIG 3**).
320 Furthermore, In this setting the staining patterns for the ATG8 family proteins LC3B and
321 GABARAP failed to indicate any notable structures. Consistent with our previous study
322 showing that UL148, but not Rh159, is sufficient to activate the UPR (10), we observed

323 accumulation of ATF4 and phosphorylated eIF2α during induction of UL148 but not
324 Rh159 (**FIG 11A**). Importantly, the intensity of HA signals detecting UL148 and Rh159
325 indicated that both ER resident immunevasins accumulate at roughly comparable levels
326 following dox induction. This argues against the possibility that gross differences in
327 induced transgene expression might account for their differing effects on UPR activation
328 and on the staining patterns for ER markers.

329 Pearson's correlation coefficient values were calculated to quantify the extent of
330 colocalization between UL148 and various cellular markers: EDEM1, Hrd1, VCP,
331 calnexin (CNX), RTN3, SEL1L, LC3B, and PDI (**FIG 11B**). The results quantitatively
332 buttress the immunofluorescent staining data shown in FIG 10. From these results, we
333 conclude that no other HCMV gene products are required for UL148 to cause ERQC
334 factors to segregate into discrete compartments. Hence, UL148 is sufficient to cause
335 large-scale reorganization of ERQC markers. Moreover, these findings suggest that
336 reorganization of ER markers into discrete structures may be related to the propensity
337 of UL148 to induce ER stress.

338 To determine whether UL148-dependent ER remodeling could be visualized in
339 real-time using live cell imaging, we constructed "tet-on" lentiviral vectors that inducibly
340 express either UL148 or Rh159 fused at their predicted C-terminal cytoplasmic tails to
341 the enhanced green fluorescent protein (GFP) from *Aequorea victoria* (32). Following
342 lentiviral transduction, puromycin-resistant ARPE-19 were isolated and subsequently
343 subjected to fluorescence-activated cell sorting (FACS) to enrich for cells that
344 expressed GFP signal following dox treatment. The resulting cell populations, which

345 inducibly express either UL148-GFP or Rh159-GFP, were designated i148^{GFP} and
346 i159^{GFP}, respectively.
347 In live cell imaging studies, we observed that the GFP signal in dox-induced
348 i148^{GFP} cells first appeared in a reticular, largely uniform pattern, which was readily
349 visible at 5 h post-induction. However, by 9 h post-induction punctate signals began to
350 appear. These puncta were observed to traffic to sites of large scale accumulation,
351 where they formed larger fluorescent structures that progressively increased in size up
352 until the termination of the experiment at 19 h (**FIG 12A, SI Movie 2**). In contrast,
353 i159^{GFP} cells exhibited a largely diffuse, reticular GFP signal at all post-dox time points
354 monitored (**FIG 12B, SI Movie 3**). The live cell imaging results therefore recapitulated
355 the differences in the HA-staining pattern that we observed between dox-induced i148^{HA}
356 and i159^{HA} cells following fixation, as well as those between HA signals during HCMV
357 infection with TB_148^{HA} and TB_159^{HA} (**FIGS 1, 3, 10, SI Fig S1**).
358
359 **UL148-GFP structures exhibit poor recovery of fluorescence after**
360 **photobleaching.**
361 To determine whether the protein contents of the UL148 induced structures
362 would exhibit decreased mobility compared to non-perturbed ER, we carried out
363 fluorescence recovery after photobleaching studies. We photobleached regions of GFP
364 signal in i148^{GFP} or i159^{GFP} ARPE-19 cells that had been induced for transgene
365 expression for 24 h and monitored recovery of fluorescence over a 5 min period. In
366 Rh159-GFP expressing cells (i159^{GFP}), fluorescence almost fully recovered within 3 min,
367 and by 5 min fully recovered to pre-bleach levels (**FIG 13D**). In contrast, when we

368 photobleached a prominent UL148-GFP structure, the GFP signal failed to appreciably
369 recover fluorescence over the 5 min period (**FIG 13E**). Nonetheless, an area of reticular
370 GFP signal in an i148^{GFP} cell that presumably represents a region of the ER not
371 involved in an anomalous structure, recovered fluorescent signal with kinetics similar to
372 those observed during Rh159-GFP expression. These results suggested to us that
373 UL148 structures do not exchange their contents as efficiently as unperturbed ER, or
374 that at least the UL148-GFP within the structures is not able to be replaced rapidly with
375 UL148-GFP fusion protein from other portions of the organelle.
376
377 **Ectopically-expressed UL148 is degraded by proteasomes and not by autophagy.**
378 The UL148 ER structures were found to be enriched with proteins such as Hrd1,
379 SEL1L, EDEM, and VCP (**FIG 3-4**, **10-11B**), which are posited to play key roles in
380 ERAD, a process during which misfolded glycoproteins are recognized, processed, and
381 dislocated across the ER membrane for degradation at cytosolic proteasomes.
382 However, we also detected elements of the machinery for autophagy in close
383 association with the UL148 structures. Namely, the mammalian ATG8 ortholog
384 GABARAP co-localized with UL148 during infection (**FIG 3-4**), and both GABARAP and
385 another ATG8 ortholog, LC3B, were found to co-localized with UL148 at the ER
386 structures during ectopic expression of UL148 (**FIG 10, 11B**). Therefore, we wished to
387 determine whether UL148 would degraded by the proteasome, as would be consistent
388 with conventional ERAD, or by the lysosome, which would suggest a role for autophagy-
389 related processes, such as selective autophagy of the ER (33), in dispensing with
390 UL148, and presumably, in resolving the ER perturbations.

391 As a first step, we conducted a live-cell imaging "washout" experiment in which
392 i148^{GFP} cells were induced for transgene expression for 24 h, after which the growth
393 medium containing the transgene inducing agent (dox) was replaced with medium
394 lacking dox. During a 22 h imaging period following dox-washout, we observed the
395 structures to become progressively smaller as the reticular and punctate GFP signals
396 gradually abated (**FIG 14A, SI Movie S7**). Because the results suggested that UL148-
397 GFP structures could be resolved over time, we induced UL148-GFP in tet-on ARPE-19
398 cells (i148^{gfp}) for 24 h, washed out the inducing agent (dox), and then applied either
399 epoxomicin (20 μM), an irreversible inhibitor of the proteasome (34), or folimycin (115
400 nM), a proton pump inhibitor that blocks autophagosome maturation and impedes the
401 lysosome-dependent protein degradation (35, 36). Of the two inhibitors, only
402 epoxomicin markedly stabilized UL148, as evidenced by the sustained Western blot
403 signal for both GFP and UL148 in this condition relative to either DMSO carrier or
404 folimycin treatments (**FIG 14B-C**). Despite that folimycin treatment had no obvious
405 effect on UL148-GFP levels, the drug markedly increased the levels of LC3B-II, as
406 would be expected with a lysosomal proton pump inhibitor. From these results, we
407 conclude that ectopically expressed UL148 is primarily degraded via a proteasome-
408 dependent mechanism.
409
410 **UL148 requires the integrated stress response to cause ER reorganization.**
411 We previously defined that UL148 triggers the UPR during ectopic expression,
412 and that UL148 contributes to activation of the PKR-like ER kinase (PERK) and inositol
413 requiring enzyme 1 (IRE1) during infection (10). Although we failed to find any effect of

414 small interfering RNA (siRNA) or drug treatments targeting IRE1 on UL148-dependent
415 ER remodeling (not shown), we did observe that siRNA directed at PERK caused
416 UL148 to fail to form puncta or to co-localize with Hrd1 (not shown). Furthermore, the
417 literature suggests that formation of ERQC compartments requires PERK (37). PERK
418 responds to ER stress by activating the integrated stress response (ISR). In particular,
419 PERK phosphorylates eIF2α at Ser51 (eIF2α-P), and the accumulation of eIF2α-P
420 causes global attenuation of mRNA translation whilst paradoxically stimulating
421 translation of select mRNAs, such as those encoding ATF4 and CHOP, which play roles
422 in adaptation to stress (38). Stress-regulated translation of such mRNAs involves small
423 upstream open reading frames (uORFs) in their 5' untranslated regions that ordinarily
424 suppress translation under basal conditions (39, 40).
425 To examine whether ER remodeling in response to UL148 requires the ISR, we
426 turned to a well characterized small molecule inhibitor of stress-regulated translation,
427 ISRIB (41-45). ISRIB is thought to function by acting as a "molecular staple" that holds
428 the guanine nucleotide exchange factor eIF2B in an active decameric configuration (43-
429 46), such that eIF2B will continue to generate ternary complex (eIF2•GTP•Met-tRNAi)
430 necessary for new cycles of translational initiation, despite the presence of phospho-
431 eIF2α (Ser51). Because PERK is the kinase that phosphorylates eIF2α in response to
432 ER stress (47, 48), we also tested for effects of the PERK inhibitor GSK2606414 (49).
433 Having confirmed that ISRIB and GSK260641 do not negatively impact UL148
434 expression during dox-induction of UL148-GFP **(FIG 15A-B)**, we treated i148^{GFP} cells
435 with 200 nM ISRIB, 1.1 μM GSK260641, or DMSO vehicle control, and carried out live
436 cell imaging during dox induction.

437 Strikingly, ISRIB and GSK6060414 virtually abolished the formation of UL148
438 puncta through 13 h post induction (dox addition), a time point at which the DMSO
439 control condition showed abundant large structures (**FIG 15C-E, SI Movies 8-10**).
440 Based on our previous findings (**FIGs 1-3, 6-7, 10)**, we interpret the formation and
441 subsequent large-scale aggregation of UL148-GFP puncta to faithfully indicate of ER
442 reorganization in response to UL148. Therefore, these results suggested to us that
443 pharmacological treatments that inhibit the ISR and PERK prevent UL148 induced
444 remodeling of the ER, which further implies that ER remodeling in response to ER
445 stress requires stress-regulated translation.
446 Since our results with ISRIB and GSK6060414 suggest that the ISR is required
447 for UL148 mediated ER remodeling during ectopic expression of UL148, we next asked
448 whether these pharmacological agents would prevent UL148-dependent ER remodeling
449 in the physiologically authentic context of HCMV infection. However, our live cell
450 imaging studies with ISRIB and GSK6060414 indicated that following a pronounced
451 delay, UL148-GFP puncta nonetheless began to appear by ~19 h post treatment (**FIG**
452 **15D-E, SI Movies 9-10**), which suggested that the pharmacological activity of the drugs
453 might diminish over time. Therefore, in order to ensure that blockade of PERK and the
454 ISR would be sustained over a four-day period that it takes for structures to fully form
455 during HCMV infection, we replenished the drugs every 24 h by replacing the spent
456 media with media containing freshly reconstituted ISRIB, GSK6060414, or DMSO
457 vehicle control.
458 At 4 days postinfection, ER structures were virtually ablated in the ISRIB and
459 GSK2606414 treatment conditions (**FIG 16A**). To quantify these effects, we obtained Z-

460 stacks from a minimum of 30 cells per treatment condition and used Imaris 3D image
461 analysis software to calculate the percentage of Hrd1 signal that coalesced into discrete
462 structures during infection. The results indicated highly significant differences between
463 the DMSO carrier alone setting compared to treatments with either GSK2606414 or
464 ISRIB (**FIG 16B**). Reassuringly, roughly equivalent levels of UL148 were detected in
465 Western blot analyses of protein extracts from drug treated and DMSO control
466 conditions, which argues against the possibility that differences in UL148 expression
467 might explain the loss of structures involving UL148 and Hrd1. Furthermore, ISRIB and
468 GSK2606414 treatments both caused reduced levels of ATF4, while PERK inhibitor
469 alone was able to reduce the levels phospho-eIF2α (Ser51), detected by a phospho-
470 specific antibody. Therefore, each of the drugs caused their expected effects on the
471 PERK / eIF2α / ATF4 axis (**FIG 16C-D**).
472 Notably, a modest reduction in the levels of the viral envelope glycoprotein B
473 (gB) was observed during treatments with ISRIB or GSK2606414. This suggests that
474 the ISR may be required for optimal expression of the certain viral envelope
475 glycoproteins. Even viruses lacking *UL148* cause high levels of ATF4 accumulation at
476 late times during infection, which is when viral late gene products, such a gB, are
477 expressed at their highest levels (10). Hence, the activity of PERK, and/or ISR
478 regulated translation may be required for optimal expression of viral envelope
479 glycoproteins. Regardless, the PERK inhibitor and ISRIB each prevented the
480 appearance of discrete UL148 ER structures while failing to substantially affect UL148
481 expression. Therefore, the effects of the two inhibitors on UL148-dependent ER
482 reorganization were fully consistent with those seen during ectopic expression of the

483 immunevasin. Taken together, our findings argue that the ISR is required for UL148 to

484 cause remodeling of the organelle.

485 **DISCUSSION**

486 The ER structures that that we have identified are noteworthy in several regards.
487 Firstly, this example of virally-induced ER remodeling is wholly dependent on a single
488 viral gene product, UL148. Of course, there are other examples of individual viral gene
489 products that are necessary to grossly perturb ER morphology during infection which
490 are also found to be sufficient to induce such perturbations [e.g., (28, 29, 50, 51)]
491 Nonetheless, to the best of our knowledge the ER structures caused by UL148 are a
492 hitherto undescribed ultrastructural characteristic of the HCMV infected cell, which is
493 surprising given their size, scale, and prominence. Indeed, the average volume of the
494 structures at 96 h postinfection amounts to roughly 60% of the size of the nucleus of an
495 uninfected human fibroblast [~500 μm^3, (52)]. Although UL148 expression is
496 accompanied by UPR activation, ER reorganization occurs without killing the host cell,
497 even in the setting of ectopic expression when viral functions that inhibit programmed
498 cell death are absent. Nor does UL148 affect the yield of infectious virus during
499 replication in fibroblasts, since *UL148*-null mutant viruses replicate indistinguishably
500 from wildtype parental virus in this cell type (1, 8). As with all enveloped viruses, HCMV
501 requires the host cell secretory pathway to fold and process enormous quantities of viral
502 envelope glycoproteins that endow progeny virions with the molecular machinery for
503 infectivity. It is intriguing to consider how the infected cell tolerates spatial
504 reorganization of ER membranes and the associated glycoprotein quality control
505 machinery without impacting the production of infectious progeny virions.

506 Furthermore, certain aspects of ER reorganization invoked by UL148 may be
507 novel to cell biology. In particular, the densely packed collapsed ER in close

508 association with varicosities that we observe to depend on UL148 during infection
509 appear to differ from the ER structures induced by other ER perturbagens. For
510 instance, a hereditary form of childhood cirrhosis caused by the *Z* allele of the alpha-1-
511 antitrypsin (Z-A1AT) gene (*SERPINA*) is characterized by polymerization of Z-A1AT
512 within the ER (25), leading to its accumulation in membrane-delimited inclusions (25,
513 26, 53). However, Z-A1AT inclusions are not observed to associate with regions of
514 collapsed ER, nor does Z-A1AT suffice to activate the UPR, even though its expression
515 sensitizes cells to other triggers of ER stress (26, 54).
516 HCMV encodes at least one other ER-resident immunevasin that activates the
517 UPR, US11 (55). UL148 binds the NK-cell and T-cell costimulatory ligand CD58 to
518 prevent its transport to the cell surface while US11 targets the heavy chain of class I
519 major histocompatibility complex (MHC) for ER-associated degradation (56, 57). UL148
520 causes CD58 to accumulate as an immature glycoform, presumably within the ER, but
521 does not lead to any obvious decrease in its overall abundance (9). Albeit that
522 intracellular forms of CD58 appear to be refractory to detection by standard indirect
523 immunofluorescence protocols (not shown), it seems reasonable to hypothesize that
524 UL148 sequesters CD58 into the unusual ER structures that it induces. Moreover, our
525 detergent solubility results suggest that UL148 may form aggregates or polymers in the
526 course of preventing CD58 presentation at the cell surface (FIG 9). It is worth noting
527 that UL148, an immunevasin targeting CD58, induces dramatic morphologic
528 rearrangements of the ER, while another HCMV immunevasin, US11, targeting MHC
529 class I for degradation evidently does not do so, even though both trigger ER stress.
530 Nonetheless, it seems unlikely that retention of CD58 would be required for ER

531 reorganization. In fact, the capacity of UL148 to retain CD58 may be functionally
532 separable from its peculiar effects on the morphology and organization of the ER.
533 Despite that the relationship between the mechanism for CD58 retention and the
534 formation of UL148-dependent ER structures remains unresolved, our findings may
535 suggest a mechanism to explain the influence of UL148 the tropism of the virus for
536 epithelial cells. These effects, which are exemplified by a ~100-fold replication
537 advantage of *UL148*-null viruses in epithelial cells, correlate with decreased expression
538 of glycoprotein O (gO) (1). We previously reported that gO behaves as a constitutive
539 ERAD substrate during infection and that immature, newly synthesized forms of gO
540 show enhanced stability in the presence of UL148 (8), and we now show that UL148
541 causes large-scale sequestration of the proteasomal ERAD factors, such as the ER
542 mannosidase EDEM1 and the E3 ubiquitin ligase SEL1L/Hrd1, into large membranous
543 structures. Collectively, these observations may suggest that regions of rough ER not
544 drawn into the structures might offer a more permissive folding environment for
545 polypeptides that are slow to fold or assemble into multiprotein complexes.
546 Indeed, our results indicate that the reticular ER, as indicated by the staining
547 pattern for calreticulin, PDI, and KDEL antibodies, remains largely intact following
548 UL148-induced ER reorganization of ER quality control markers into discrete structures.
549 Based on these findings, we hypothesize that UL148 alters ER proteostasis by
550 physically dislocating key elements of the “mannose removal time clock” system that
551 marks poorly folding glycoproteins for destruction via ERAD (58, 59). Because gO is
552 both the defining subunit of the heterotrimeric gH/gL/gO envelope glycoprotein complex
553 that governs HCMV entry and cell tropism (5-7, 60, 61), and a constitutive ERAD

554 substrate (1, 8), the hypothesis that ER reorganization is required for the effects of
555 UL148 on HCMV cell tropism does not seem unreasonable on its face. Going forward,
556 it will be crucial to determine whether classical ERAD substrates, such as the null Hong
557 Kong variant of alpha-1-antitrypsin (62, 63) or ribophorin-332 (64, 65), are stabilized
558 during UL148 expression, as would be predicted if UL148 shifts ER proteostasis to
559 negatively modulate ERAD.

560 In addition to having found that factors involved in proteasomal ERAD, such as
561 Hrd1 and EDEM1, are enriched at the UL148 structures, we also observed that
562 GABARAP, a mammalian ortholog of yeast ATG8, localizes to the UL148 ER structures
563 during infection, and that another ATG8 ortholog, LC3B, and GABARAP both associate
564 with the structures during ectopic expression of UL148. This may suggest roles for
565 autophagy-related pathways in UL148-dependent reorganization of the organelle.
566 Since our results indicate that UL148 is degraded by a proteasome-dependent pathway
567 and not by lysosomes, it seems unlikely that selective autophagy of the ER is directly
568 involved in recycling or degrading these ER structures. Nonetheless, ATG8 family
569 proteins may contribute to formation of large structures, vis-a-vis the trafficking of
570 UL148-GFP puncta observed during our live cell imaging studies. Previous work
571 indicates that misfolded proteins traffic in a microtubule (MT)-dependent manner to form
572 pericentriolar structures termed aggresomes (66, 67). ATG8 family proteins such as
573 LC3B and GABARAP not only play roles in degradation of substrates via
574 macroautophagy, but also bind MTs and recruit machinery for MT-dependent transport
575 of cargos (68-70). Therefore, GABARAP and LC3B may be important for the

576 recruitment of cellular machinery that transports perturbed ER cargoes to sites of large-
577 scale accumulation.

578 Although that our results argue that the ISR is required for ER reorganization
579 during UL148 expression, precisely how UL148 triggers ER stress remains unknown.
580 UL148 has been found to co-purify from cells with SEL1L, a component of the ERAD
581 machinery. Thus, it seems plausible that UL148 may inhibit the Hrd1/SEL1L complex,
582 which would cause the buildup of unfolded proteins and thus trigger the UPR. However,
583 inhibition of ERAD in and of itself seems unlikely to account for the formation of ER
584 structures. Another non-mutually exclusive possibility is that UL148 multimerizes or
585 aggregates in a manner that constricts the ER lumen. For instance, the assembly of
586 UL148 molecules on opposite sides of the ER lumen might constrict the organelle in a
587 manner consistent with the collapsed regions of ER observed in our EM results (FIGS 6,
588 8).

589 Despite that additional work will certainly be needed to decipher the molecular
590 mechanisms by which UL148 causes reorganization of the ER, and to determine its
591 physiological relevance to viral biology. Nonetheless, we have shown that UL148, when
592 fused to a fluorescent protein, suffices to trigger and robustly indicate the ISR (FIGS 15-
593 16), which suggests that UL148 could be used in screens to identify novel inhibitors of
594 the ISR, as well as in genetic screens to identify cellular genes involved in stress-
595 dependent remodeling of the ER. Interestingly, the two pharmacological agents that we
596 have identified to block UL148-dependent ER remodeling, ISRIB and GSK2606414, are
597 also known to disperse stress granules (SGs) and to prevent their formation in the first
598 place. SGs are comprised of condensed aggregates of protein and RNA that occur due

599 to stalled mRNA translation in disease states, such as amyotrophic lateral sclerosis
600 (71), and during treatments with toxic agents such as arsenite (42, 72). It is fascinating
601 to consider that mechanistic parallels exist between the formation of SGs and the
602 UL148-dependent reorganization of the ER. Moreover, given the broad importance
603 macromolecular aggregation in pathological conditions such as neurodegenerative
604 diseases (73), certain of which also involve defects in ER proteostasis and aberrant
605 activation of the UPR, UL148 may hold promise as tool to discover new agents to
606 ameliorate disease.
607

608 **MATERIALS AND METHODS.**

609

610 **Cells and Virus.**

611 hTERT-immortalized human foreskin fibroblasts (8), derived from ATCC HFF-1 cells
612 (SCRC-1041) were maintained in Dulbecco's modified Eagle's medium supplemented
613 with 5%-10% newborn calf serum (Millipore Sigma) and antibiotics (complete DMEM)
614 exactly as described previously (8). i148^{HA} and i159^{HA} ARPE-19 epithelial cells (10),
615 which upon treatment with 100 ng/mL doxycycline, express HA-tagged UL148 or
616 Rh159, respectively, were likewise maintained in complete DMEM. For live cell imaging
617 studies, i148^{HA} and i159^{HA} ARPE-19 were maintained in Opti-MEM (Thermo Fisher)
618 supplemented with 3% certified tet-approves fetal bovine serum (FBS), 20 µg/mL
619 gentamicin sulfate, 1 µg/mL puromycin HCl and 10 µg/mL ciprofloxacin HCl.
620 Telomerase-immortalized rhesus fibroblasts (74) were a kind gift of Peter A. Barry, and
621 were maintained in complete DMEM. The acute monocytic leukemia cell line THP-1
622 (TIB-202) was obtained from ATCC (Manassas, VA) and were maintained in RPMI 1640
623 medium supplemented with 10% FBS (Millipore Sigma) and antibiotics (10 µg/mL
624 ciprofloxacin and 25 µg/mL gentamicin). THP-1 were differentiated into adherent
625 macrophages by incubating for 48 h in the presence of 100 nM 2-O-
626 tetradecanoylphorbol 13-acetate (Millipore Sigma), and subsequently infected with the
627 indicated viruses at an MOI of 5 $TCID_{50}$/cell.

628 Infectious bacterial artificial chromosome (BAC) clones of the following HCMV
629 strains were used for this study: TB40/E (also known as TB40-BAC4 or TB_WT) (75)
630 as well as its derivatives TB_148^{HA} and TB_148$_{STOP}$, which were used in our previous

631 studies (1, 8, 10); TR (TR*gfp*)(76, 77); Merlin repaired for *UL128* and *RL13* harboring
632 *tetO* sequences upstream of *UL131* (pAL1393) (78); AD169 repaired for *UL131*
633 (AD_r131)(1, 79) and AD_r131_148^{HA}, a derivative of AD_r131 that carries a full length
634 UL148 (from strain TB40/E) tagged with an HA-epitope at the original *UL148* locus (8).
635 An infectious BAC clone of rhesus CMV (RhCMV) strain 68-1 (80) and a derivative that
636 expresses an HA-tagged Rh159 (details below) were also used for certain experiments.
637 The methods used for reconstitution of HCMV from purified BAC DNA, cultivation
638 of virus and preparation of stocks, including ultracentrifugation through sorbitol cushions
639 and determination of infectious titers by tissue culture infectious dose 50 ($TCID_{50}$) assay
640 have been described elsewhere (8, 10).
641
642 **Construction of recombinant viruses and recombinant DNAs.**
643 New recombinant viruses for this study were derived from BAC-cloned HCMV
644 and RhCMVs using *en passant* mutagenesis in GS1783 *E. coli,* a strain K12 derivative
645 that expresses the homing endonuclease I-SceI upon treatment with L-(+)-arabinose
646 (81, 82). Recombinant BACs were confirmed by Sanger DNA sequencing of the
647 modified regions, which was performed by Genewiz, Inc. (Piscataway, NJ) (not shown).
648 Oligonucleotide primers for construction of recombinant viruses and plasmids were
649 custom synthesized by Integrated DNA Technologies (Coralville, IA); sequences are
650 provided in **Table S1**. Type II restriction endonucleases, T4 DNA ligase, and Gibson
651 assembly reagents (NEB HiFi Assembly Master Mix) for generation of recombinant
652 DNAs and for routine molecular cloning and subcloning procedures were obtained from

653 New England Biolabs (Ipswitch, MA). KOD Hot Start DNA polymerase (EMD Millipore)
654 was used for all PCR reactions.
655 To construct TB_159^{HA}, a strain TB40/E derivative in which the UL148 open
656 reading frame is replaced by Rh159 we carried out the following steps. Primers
657 Rh159_Fw and Rh159_HA_Rv were used to amplify and HA-tag the *Rh159* ORF from
658 pcDNA3.1+_Rh159_IRES_GFP (a gift from Klaus Früh, OHSU). The PCR product was
659 inserted into EcoRV-digested pEF1α using Gibson assembly. A PCR product
660 containing an ISce-I excisable kanamycin cassette was amplified from TB_148^{HA}_*ISce-*
661 *Kan* integrate BAC (1) using primers PpuISceKanGibs_Fw and PpuISceKanGibs _Rv
662 and Gibson-assembled into PpuMI-digested pEF1α_Rh159 plasmid to yield plasmid
663 pEF1α_Rh159_ISceKan. Primers Rh159_Fw_recomb and Rh159_Rv_recomb were
664 used to generate a PCR product from template plasmid pEF1α_Rh159_ISceKan. The
665 PCR product was electroporated into GS1783 E. coli harboring the TB_148^{HA} BAC, and
666 Kan^r colonies harboring TB_Δ148_Rh159_ISceKan integrate BACs were isolated on
667 Luria-Bertiani agar plates. Bacterial colonies representing Kan resistant integrates were
668 obtained, and integrates were subsequently resolved using standard *en passant*
669 protocols to yield TB_Δ148_Rh159^{HA}, which we abbreviate herein as TB_159^{HA}.
670 TB_159^{HA} was sequence-confirmed using primers TB_Rh159HA_seq_Fw and REV
671 TB_Rh159HA_seq. Similar strategies were used to modify the RhCMV 68-1 BAC (80)
672 so as to insert sequences encoding the nonapeptide HA-epitope such that Rh159 would
673 be expressed from the virus carrying a C-terminal HA tag. An *en passant* strategy in
674 which a shuttle plasmid carrying *I-SceI-Kan^r* disrupted by in-frame nonsense codons
675 was used insert premature nonsense codons in the *UL148* CDS in the context of HCMV

676 strains Merlin (pAL1393) and TR (TR*gfp*), and was applied as described previously for
677 generating TB_148$_{STOP}$, the UL148$_{STOP}$ mutant of strain TB40/E (8).
678 To construct "tet-on" lentivirus vector plasmids containing UL148 fused to GFP,
679 we used primers Gibs_eGFP_Rv and 148_eGFP_Fw to amplify the GFP gene from a
680 dsDNA gBlock, EGFP-P2A-3XHA, synthesized by Integrated DNA Technologies, gift of
681 Matthew D. Woolard, LSUHSC-S. In a separate PCR, the *UL148* gene was amplified
682 from plasmid pcDNA3.1-UL148^{HA} (10) using primers Gib_148_Fw
683 148_noStopRv. The two products were assembled together with EcoRV opened
684 pcDNA3.1(+) (Invitrogen) to produce pcDNA3.1-UL148-GFP. After confirming the
685 absence of spurious mutations by Sanger DNA sequencing (Genewiz), the *UL148-GFP*
686 cassette from pcDNA3.1-UL148-GFP was released by EcoRI and NotI digestion and
687 ligated into pOUPc turboRFP-link plasmid which had been linearized using the same
688 restriction sites. pOUPc turboRFP-link is a derivative of lentiviral vector pOUPc (10)
689 that was constructed by reinsertion of turboRFP (tRFP). Briefly, tRFP was amplified
690 from the original pOUPc-turboRFP using primer pair tRFP linker Fw and tRFP linker Rv
691 and then reinserted by Gibson Assembly with pOUPc turboRFP that had been double-
692 digested using EcoRI and Not I in order to linearize the vector and remove the
693 *turboRFP* (RFP) sequence. To express Rh159 fused to eGFP, primers Gibs_eGFP_Rv
694 and 159_eGFP_Fw were used to amplify the GFP gene from EGFP-P2A-3XHA, and in
695 a separate PCR reaction, primers Gibs_159_Fw and 159_noStop_Rv Rh159 were
696 used to amplify *Rh159* from pcDNA3.1-Rh159^{HA} (10). The latter two PCR products were
697 assembled together with EcoRV linearized pcDNA3.1(+) using Gibson Assembly,
698 resulting in plasmid pcDNA3.1-Rh159. The latter plasmid was used as template in a

699 PCR reaction with primers Gibs_Age_159_Fw and Gibs_Mlu_GFP_Rv. The resulting
700 PCR product was Gibson assembled into the lentiviral vector pOUPc (10) which had
701 been double-digested with Mlu I and Age I.
702
703 **Drug treatments.**
704 The PERK inhibitor, GSK2606414 (49), doxycycline hyclate, and folimycin were
705 obtained from MilliporeSigma (Burlington, MA). ISRIB (41-45) was obtained from
706 MilliporeSigma or APExBio (Boston, MA) and epoxomicin was procured Selleck
707 Chemicals (Houston, TX). ISRIB was dissolved in DMSO to make a 10,000× stock
708 solution (2 mM) and used at a final working concentration of 200 nM. GSK2606414 was
709 dissolved in DMSO to make a 10,000× stock solution (11 mM) and used at a final
710 working concentration of 1.1 μM. Folimycin was prepared as a 1000× (115.46 μM)
711 stock solution in DMSO and used at 115 nM final. Epoxomycin was prepared as a 100×
712 (2 mM) stock solution in DMSO and used at a final concentration of 20 μM.
713
714 **Confocal Microscopy and Live Cell Imaging.** Confocal indirect immunofluorescence
715 microscopy imaging on fixed cells was carried out using Leica TCS SP5 Spectral
716 Confocal Microscope (Leica Microsystems, Heidelberg, Germany) using a Leica HCX
717 PL APO CS 63x/1.4-0.6NA objective under oil immersion, except for the image shown
718 in Figure 1C, which was captured on a Nikon SIM-E and A1R confocal microscopy
719 system (Nikon Instruments, Melville, NY) using a Nikon SR Apo TIRF 100x/1.49NA
720 objective under oil immersion. Images for different fluorophore channels were acquired
721 using sequential scanning. Direct immunofluorescence live cell imaging data were

722 collected using the Nikon SIM-E microscope using a Nikon Apo 60x/1.40NA DIC
723 objective.
724 The 3D projections shown in FIGs 1D and 16A were generated from Z-stacks
725 captured on the Nikon SIM-E / A1R microscope using a Nikon SR Apo TIRF
726 100x/1.49NA objective. For FIG 1D, the 3D projection was generated using NIS-
727 Elements AR Analysis 4.60.00 (64-bit) software (Nikon). For FIG 16A, 3D projections
728 were generated by Imaris x64 9.3.0 software (Bitplane, Inc.) in maximum intensity
729 projection (MIP) mode.
730 For fixed cell imaging experiments other than those shown in Fig S1 panels E, F,
731 G, and H, cells were seeded on 12 mm circular, No. 1 thickness microscope cover glass
732 (200121; Azer Scientific, Morgantown, PA). At the indicated times post-treatment and or
733 post-infection, cells were washed with phosphate buffered saline (PBS) [137 mM NaCl,
734 2.7 mM KCl, 10 mM Na_2HPO_4, and 1.8 mM KH_2PO_4, pH 7.4]; fixed for 15 min at room
735 temperature in PBS containing 4% (wt/vol) paraformaldehyde (Fisher Scientific, Waltham,
736 MA), washed in PBS, permeabilized for 10 min using 0.1% Triton X-100 (in PBS),
737 subsequently washed again in PBS, and then blocked for 45 min at 37 °C in PBS
738 containing 5% (vol/vol) normal goat serum (Rockland Immunochemicals, Limerick, PA).
739 Cells were then washed three times in PBS followed by incubation in 1% Human Fc Block
740 (BD Biosciences, San Jose, CA) in PBS, for additional 45 min at 37 °C. Cells were then
741 incubated in the presence of primary antibodies for 1 h at 37 °C or 4 °C overnight, and
742 then washed three times with PBS containing 0.1% Tween-20 (PBST) for 5 min per wash.
743 Alexa Fluor-labeled goat polyclonal secondary antibodies (all from ThermoFisher
744 Invitrogen, Waltham, MA, see **Table S2**) were used for secondary detection. The slides

745 were then mounted using Prolong Gold anti-fade reagent containing DAPI
746 (ThermoFisher) and placed under a Leica TCS SP5 confocal microscope for image
747 acquisition using a Leica 63× oil immersion objective lens (Leica Microsystems, Buffalo
748 Grove, IL).

749 For indirect immunofluorescence staining results of primary clinical isolates (SI Fig
750 S1 panels E-H), four clinical HCMV isolates obtained by routine testing of throat swabs
751 from patients of the Ulm University Medical Center were provided by the diagnostic
752 laboratory of the Institute of Virology in Ulm. Sample material was applied to human
753 fibroblasts and incubated for several days until HCMV-positive cells could be detected.
754 Infected cells were then seeded together with uninfected fibroblasts, incubated for up to
755 5 days until plaques were formed and processed for indirect immunofluorescence
756 staining. ERQC compartments were detected by staining for calnexin (CNX, E10; Santa
757 Cruz Biotechnology, mouse, 1:50 dilution), the cVAC was detected by staining for HCMV
758 pUL71 (rabbit, 1:500). Secondary antibody used for detection of CNX was Alexa Fluor
759 555 labeled goat anti-mouse IgG (1:1000) and for pUL71 detection, Alexa Fluor 488
760 conjugated goat anti-rabbit IgG (1:1000). Confocal images were acquired using the 63×
761 objective of a Zeiss Observer Z1 fluorescence microscope equipped with Apotome and
762 Zen software 2.3 (Carl Zeiss Microscopy GmbH, Jena, Germany).

763

764 **FRAP.** FRAP studies were carried out on using live ARPE-19 cells from the i148^{GFP}
765 and i159^{GFP} populations as follows. Cells were seeded as above for live-cell imaging,
766 induced for transgene expression using dox (100 ng) for 24 h, and then placed on an
767 incubated sample stage of a Nikon A1R SIM-E imaging system equipped with an SR

768 Apo TIRF 100x/1.49NA objective (Nikon). Three rectangular regions in image fields
769 were defined for measurement of (i) background signal, and of two regions with
770 comparable initial GFP signals, (ii) one designated as a control region (no
771 photobleaching) and another for (iii) photobleaching and recovery of signal after
772 photobleaching. Photobleaching of selected regions was carried out for 20 s using 405
773 nm laser light from a LU-N4 laser fiber (Nikon) [power at source: 15 mW, at objective: 8
774 mW]. Images and signal intensity measurements were captured every 2 s at a rate of 1
775 frame per s (488 nm excitation, FITC channel) starting immediately before
776 photobleaching (t=1), and from t=20 s to t=320 s after.
777
778 **Electron Microscopy.** Procedures to prepare samples for transmission electron
779 microscopy (TEM) included high-pressure freezing (HPF), freeze substitution, and Epon
780 embedding, which were carried out as described previously (83). Briefly, human
781 fibroblasts were seeded in μ-Slides (Ibidi GmbH, Martinsried, Germany) containing
782 carbon-coated sapphire discs (Engineering Office M. Wohlwend GmbH) 1 day prior to
783 infection at 80 to 90% confluence. Cells were infected with virus overnight at MOI 1.
784 Medium containing viral inocula was replaced with fresh medium the next day. Infected
785 cells on sapphire discs were fixed by using HPF with a Compact 01 high-pressure freezer
786 (Engineering Office M. Wohlwend GmbH, Sennwald, Switzerland) at 5 dpi. Thereafter,
787 cells on sapphire discs were processed by freeze-substitution and subsequently
788 embedded in Epon (Fluka, Buchs, Switzerland). Ultrathin sections of the Epon-embedded
789 cells were cut with an ultramicrotome (Ultracut UCT; Leica Microsystems, Wetzlar,
790 Germany) and placed on Formvar-coated single-slot grids (Plano GmbH, Wetzlar,

791 Germany). Grids were examined in a Jeol JEM-1400 (Jeol Ltd., Tokyo, Japan)
792 transmission electron microscope equipped with a charge-coupled-device (CCD) camera
793 at an acceleration voltage of 120 kV. Fixation and embedding of infected cells for
794 scanning transmission electron microscopy (STEM) tomography was the same as
795 described for TEM. Additional sample preparation steps were conducted as described
796 previously (84, 85). Tomogram acquisition was conducted on a STEM Jeol JEM-2100F
797 with an acceleration voltage of 200 kV. Tilt series were acquired from 600 nm thin
798 sections from +72° to -72° with a 1.5° increment using the bright field detector. Image
799 series were reconstructed to tomograms by weighted back projection with the IMOD
800 software package (86). Three-dimensional visualization of the membrane structures was
801 performed using Avizo lite software (Visualization Science Group, Burlington, MA, USA)
802 by threshold segmentation.
803
804 **Western blotting.** Western blotting procedures, including primary and secondary
805 antibodies used for detection of HA tag, ATF4, eIF2α, P-eIF2α (Ser51), the HCMV viral
806 nuclear antigen IE1, and the conditions used for detection of Ser51 phosphorylated
807 eIF2α, were carried out as described previously (8, 10). Additional antibodies used in
808 this study were mouse anti-GAPDH (Cat. No. 60004-1, Proteintech, Rosemont, IL,),
809 mouse anti-gB clone 27-180 (87) (a generous gift of William J. Britt), and anti-GFP
810 (D5.1) XP® Rabbit mAb #2956 (Cell Signaling Technology, Danvers, MA).
811
812 **Solubility analyses.** 2.0×10^5 human fibroblasts were infected at an MOI of 1 $TCID_{50}$
813 per cell with TB_148^{HA} or TB_159^{HA}. The following day, cells were washed twice with

814 PBS to remove viral inoculum and replenished with DMEM containing 5% newborn calf
815 serum. At the indicated times post-infection, cells were washed once with PBS and
816 lysed by direct addition of 100 μL RIPA buffer [25 mM HEPES (pH 7.5), 400 mM NaCl,
817 0.1% SDS, 0.5% sodium deoxycholate, 1% NP-40, supplemented with 1× protease
818 inhibitor cocktail (ApexBio)]. Lysates were collected and rotated at 4˚C for 1 h.
819 Insoluble material was pelleted by centrifugation (21,000 × *g*, 35 min). Supernatants
820 containing soluble material were transferred to a fresh microfuge tube, and 33 μL of 4×
821 Laemmli sample buffer [200 mM Tris (pH 6.8), 8% SDS, 40% glycerol, 0.08%
822 bromophenol blue] was added to bring final volume to 133 μL. The pellet was disrupted
823 in 133 μL of 1X Laemmli buffer prepared by diluting 4× Laemmli buffer in RIPA buffer.
824 Samples were reduced by addition of beta-mercaptoethanol (5% final, v/v) and boiled at
825 90˚C for 10 min. 40 μL of each sample was resolved by SDS-PAGE (12%
826 polyacrylamide gel), transferred overnight to nitrocellulose membrane, and
827 immunoblotted with antibodies against HA epitope or HCMV gB. Quantitation of
828 secondary antibody fluorescence signals were performed using an Odyssey CLx
829 scanner (Li-Cor, Inc., Lincoln, NE) in auto-scan mode. For each time-point, the signals
830 from RIPA-soluble and insoluble bands were summed to yield total signal, and the ratio
831 of insoluble band signal to total signal were also reported as percent insoluble HA over
832 total HA signal.
833
834 **Statistical analyses.** Statistical analyses were carried out using GraphPad Prism 8.1.0
835 for MacOS (GraphPad, Inc., San Diego, CA).
836

837 **ACKNOWLEDGEMENTS.**

838 This project was supported by NIH grants R01-AI116851 (to J.P.K.) and P30-
839 GM110703. Its contents are solely the responsibility of the authors and do not
840 necessarily represent the official views of the NIAID or the NIGMS.

841 We are especially grateful to Erik L. Snapp (HHMI, Janelia Laboratories) for
842 helpful discussions concerning interpretation of EM and confocal image data. We also
843 thank Jacob E. Corn and Jin Rui "Amos" Liang (both of ETH Zurich, Switzerland), Dong
844 Yu (Washington University, St. Louis, MO, currently GSK Vaccines), Thomas E. Shenk
845 (Princeton University, Princeton, NJ), Richard J. Stanton (Cardiff University, United
846 Kingdom), William J. Britt (University of Alabama, Birmingham), W. L. William Chang
847 and Peter A. Barry (both of the University of California, Davis; Davis, CA), Christian
848 Sinzger (University Medical Center Ulm, Ulm, Germany), Klaus Früh (Oregon Health
849 Sciences University, Beaverton, OR), and Gregory A. Smith (Northwestern University,
850 Chicago, IL) for generously sharing reagents.

851

852 **AUTHOR CONTRIBUTIONS.**

853 Performed experiments: HZ, CR, CCN, MNAS, JvE. Data analysis and interpretation:
854 HZ, CR, CCN, JvE, CS, JPK. Wrote the manuscript: JPK with comments from JvE and
855 CR. Conceived of the study: JPK. Designed experiments: HZ, JvE, CR, CCN.
856 Contributed new reagents: HZ, CH, CCN, JPK. Electron microscopy: CR and JvE.
857 Protein solubility analysis: CCN. Obtained funding: JPK.

858 HZ performed all confocal immunofluorescence experiments with the exception of the SI
859 Figure on primary clinical isolates from patient throat swabs (JvE), viral replication kinetics

860 experiments, and also constructed novel reagents, including lentivirus vector plasmids for
861 isolating i148-GFP and i159-GFP ARPE-19 cell populations. HZ also carried out FRAP
862 studies, and performed all of the live cell imaging experiments, and all Western blots in
863 the study, except those otherwise specified below. CR carried out the TEM and STEM
864 tomography studies. CCN constructed the TB_159^{HA} virus and conceived of and
865 performed the protein solubility analyses comparing UL148 and Rh159. MS carried out
866 Western blotting studies on the effects of folimycin versus epoxomicin on UL148
867 degradation. CH constructed the RhCMV 68-1 BAC carrying an HA-tagged Rh159. CS
868 assisted with confocal imaging and with Imaris and Nikon software analyses of the 3D
869 images.
870

871 **FIGURE LEGENDS:**

872

873 **FIG 1. UL148 reorganizes ER markers into anomalous structures during HCMV**
874 **infection.**

875 Fibroblasts infected at 1 MOI with either **(A)** wildtype HCMV strain TB40/E (TB_WT) or
876 **(B)** an isogenic *UL148*-null mutant (TB_148_{STOP}), were fixed at 96 h postinfection (hpi)
877 and imaged by confocal microscopy after staining with antibodies specific for calnexin or
878 Hrd1 (magenta) and glycoprotein H (gH, green), as indicated. DAPI (blue) signal was
879 used to counterstain nuclei. **(C)** Percentage of fibroblasts that contain Hrd1 structures at
880 96 hpi; fifty gH-positive cells for each condition were scored for the presence or absence
881 of UL148 structures (also see SI Fig S1A). (**D**) Three-dimensional confocal image
882 projection of a TB_WT infected fibroblast stained at 96 hpi for Hrd1 and gH. **(E)**
883 Volumetric measurements were made from sixteen infected cells, stained with phalloidin-
884 AlexaFluor 594 conjugate to estimate total cell volume, with Hrd1 antibody to estimate
885 the volume of UL148-dependent ER structures, and with DAPI to estimate nuclear
886 volume.

887

888 **FIG 2. Characterization of TB_148^{HA} and TB_159^{HA} viruses. (A)** Human fibroblasts
889 were infected at MOI 1 with the indicated recombinant HCMVs and whole cell lysate
890 samples harvested at the indicated times post-infection (h post-infection: hpi) were
891 analyzed by Western blot to detect HA-tagged UL148 or Rh159, the 72 kD viral nuclear
892 antigen IE1-72 (IE1), and GAPDH. **(B)** Single-cycle viral replication kinetic curves from

893 MOI 1 infected fibroblasts were plotted by determining the titer in tissue culture infectious
894 dose 50 ($TCID_{50}$) from supernatants collected at the indicated times postinfection.
895
896
897 **FIG 3. UL148 localizes to unusual ER compartments enriched for glycoprotein**
898 **quality control markers.** Fibroblasts infected at MOI 1 with either TB_148^{HA} (panels: **A,**
899 **C, E, G, I, K, M, O, Q, S**) or TB_ 159^{HA} (panels: **B, D, F, H, J, L, N, P, R, T**) were fixed
900 at 96 hpi, and imaged by confocal microscopy after co-staining with antibodies specific
901 for HA (UL148/Rh159, magenta in merge) and the indicated cellular markers (green in
902 merge). DAPI (blue) counterstaining is shown in merged image.
903
904 **FIG 4. Quantification of Co-localization between UL148 and Cellular Markers.** A
905 Pearson's correlation coefficient (*r*) was calculated using NIH ImageJ software to estimate
906 the degree of co-localization between UL148 (HA signal) and each of the indicated
907 cellular markers. A minimum of 30 cells were analyzed per marker. The arithmetic mean
908 for each co-localization analysis result is shown as a blue line, and data points for
909 individual cells analyzed are plotted as circles.
910
911 **FIG 5. Cellular proteins involved in glycoprotein quality control are recruited with**
912 **differing kinetics to UL148 ER structures.** Fibroblasts infected with TB_148^{HA} at 1 MOI
913 were fixed at the indicated time points (days post infection, dpi) and imaged by confocal
914 microscopy after staining with antibodies specific for HA (UL148, magenta), CNX (green,
915 **A**) , Hrd1 (green, **B**) or VCP(green, **C**), DAPI (blue).

916

917 **FIG 6. TEM of ER structures in wild-type HCMV infected cells.** Human fibroblasts
918 infected with wildtype HCMV (TB_WT) were fixed by high-pressure freezing and freeze
919 substitution at day 5 postinfection and imaged using TEM. Panels (**A**) and (**B**) show cell
920 overview at left. For each cell, the boxed region is shown at higher magnification.
921 Scale bars; left panels: 10 µm, right panels: 2 µm. rER: rough ER; Nu: nucleus; cVAC:
922 cytoplasmic viral assembly compartment. Solid arrowheads indicate the UL148-
923 dependent ER structures of interest.

924

925 **FIG 7. TEM of *UL148*-null HCMV infected cells.** Human fibroblasts infected with a
926 *UL148*-null mutant (TB_148$_{STOP}$) were fixed by high-pressure freezing and freeze
927 substitution at day 5 postinfection and imaged using TEM. At the upper left an overview
928 panel of a representative cell is shown with panels **A, B, and C** each boxed. The boxed
929 regions are expanded at higher magnification at right (**A**) and below (**B, C**). Scale bars
930 for upper left overview panel: 10 µm, for zoomed panels: 2 µm. rER: rough ER; Nu:
931 nucleus; cVAC: cytoplasmic viral assembly compartment.

932

933 **FIG 8. STEM tomography of UL148-dependent ER structures in HCMV infected**
934 **cells.** Human fibroblasts infected with wildtype HCMV (TB_WT) were fixed by high-
935 pressure freezing and freeze substitution at day 5 postinfection and tomograms were
936 recorded by STEM. (**A**) Shows a virtual section through the tomogram of a virus-
937 induced membranous structure; asterisks denote ER structures of distended lumenal
938 space. White arrowheads indicate sites at which membranes originating from distended

939 ER cisternae continue into areas of involuted collapsed ER. Scale bar: 1 μm. (**B**)
940 Shows the same virtual section as in (A) tilted and with a 3D visualization of the
941 membranous network (green) of the entire tomogram. The same distended ER
942 cisternae as in (A) are marked by asterisks. (**C**) Shows a cross section through (B) to
943 visualize the membrane profile of the membranous structures. The region delimited by
944 a white box is shown in a higher magnification on the right. Finer detail of the enlarged
945 ER cisternae and the connections between them are readily visible; asterisks indicate
946 the same distended ER cisternae as in (A) and (B). Also, see SI Movie S1. Scale bar: 1
947 μm.
948
949 **FIG 9**. Solubility Analysis of UL148 and Rh159. (**A**) Human fibroblasts were infected at
950 MOI 1 $TCID_{50}$/cell with HCMV strain TB40/E derived viruses TB_148^{HA}, which
951 expresses UL148 fused at its C-terminus to an HA-epitope tag, or TB_159^{HA}, which
952 lacks *UL148* and instead expresses rhesus CMV Rh159 carrying a C-terminal HA tag.
953 At the indicated times postinfection (hpi), infected cells were collected
954 radioimmunoprecipitation (RIPA) lysis buffer, centrifuged at 21,000×g for 30 min, after
955 which supernatant (sup) and pellet (pel) fractions were boiled in gel loading buffer
956 containing 2% sodium dodecyl sulfate (SDS). Equivalent portions of supernatant and
957 pellet were resolved by SDS-polyacrylamide gel electrophoresis, transferred to a
958 nitrocellulose membrane for detection of protein species immunoreactive to antibodies
959 against HA epitope (HA) and HCMV glycoprotein B (gB) and for total protein signal
960 using Ponceau S reagent (Ponceau). (**B-C**). Signal intensity of fluorophore-conjugated
961 secondary antibodies in anti-HA Western blots were measured from three independent

962 biological replicates of the experiment shown in (A); error bars indicate standard
963 deviation. (**B**) The fluorescent signal for each infection time point condition (Y-axis
964 indicates arbitrary units, in hundred thousands). (**C**) The amount of signal found in the
965 insoluble (pellet) fraction relative to the total signal (pellet plus supernatant) for each
966 infection time point are plotted as percentage values.
967
968 **FIG 10. UL148 is sufficient to remodel the ER.** HA-tagged UL148 or Rh159 were
969 doxycycline (dox) induced in the context of a "tet-on" lentiviral vector system in stably
970 transduced ARPE-19 epithelial cell populations, i148^{HA} and i159^{HA}, respectively. Cells
971 were fixed at 48 h postinduction for indirect immunofluorescence staining for the
972 indicated cellular markers (green) together with HA (magenta). Scale bar: 10 μm.
973
974 **FIG 11. ISR activation accompanies redistribution of ER markers during ectopic**
975 **expression of UL148. (A)** Lysates of tet-on ARPE-19 cells expressing either UL148 or
976 Rh159 fused to an HA tag, i148HA and i159HA, respectively, were collected at the
977 indicated times post doxycycline (dox) induction and analyzed by Western blot for the
978 expression of the indicated proteins and for the abundance of eIF2α phosphorylated at
979 Ser51 (P-eIF2α) using a phospho-specific antibody. (**B**) Pearson's correlation
980 coefficient (*r*) values were calculated using NIH ImageJ software estimate the degree of
981 co-localization between UL148 (HA signal) and the indicated cellular markers. A
982 minimum of 30 cells were analyzed per marker. Arithmetic means for each co-
983 localization analysis result are shown as blue lines, and data points for individual cells
984 analyzed are plotted as circles.

985

986 **FIG 12. Live Cell Imaging of UL148-GFP and Rh159-GFP during Induced Ectopic**
987 **Expression.** "Tet-on" ARPE-19 epithelial cells that inducibly express either UL148 or
988 Rh159 fused to green florescent protein (gfp), i148^{gfp} (**A**) and i159^{gfp} (**B**), respectively,
989 were induced for transgene expression using 100 ng/mL doxycycline (dox) and imaged
990 using live-cell microscopy. Images from the selected time points (h post treatment with
991 dox, hpt) are shown. The main scale bar represents 50 µm. For inset panels at upper
992 left of each image, which are magnified 2.4× relative to the main image, the scale bar
993 represents 10 µm. Also see SI Movies S2-S3.

994

995

996 **FIG 13. FRAP analysis.** ARPE-19 cells that inducibly express Rh159-GFP, i159^{gfp} (**A**)
997 or UL148-GFP, i148^{gfp} (**B-C**) were doxycycline induced for 24 h (100 ng/mL doxycycline
998 (dox). Separate regions of GFP signal in selected cells were photobleached (405 nm
999 laser) or left unbleached, while a third region lacking GFP signal was chosen as a
1000 background reference were measured before and during fluorescence recovery after
1001 photobleaching (FRAP). Note: background signal was not plotted because values were
1002 resolvable from the x-axis. GFP signal intensity is plotted over a time period (seconds,
1003 s) starting with an exposure at t=0 (immediately before photobleaching), and including
1004 measurements taken every 2 s after photobleaching (0-20 s) until termination of the
1005 measurement series at t=322 s (300 s of FRAP). (**D-F**) Images from the selected time
1006 points (s, seconds) immediately before and after bleaching, and during fluorescence
1007 recovery period. Also see SI Movies S4-S6.

1008

1009 **FIG 14: UL148-GFP is stabilized by inhibition of proteasomal but not lysosomal**
1010 **degradation.** "Tet-on" ARPE-19 cells that inducibly express UL148-GFP (i148^{gfp}) were
1011 induced for 24 h by the addition of 100 ng/mL doxycycline (dox), after which the dox
1012 inducing agent was washed out and medium containing either the proteasome inhibitor
1013 epoxomicin (20 μM) or the proton pump inhibitor folimycin (115 nM) was added and
1014 samples were harvested for Western blot analysis at the indicated times post treatment
1015 (h post treatment, hpt) with folimycin or epoxomicin. Also see SI Movie S7.

1016

1017

1018 **FIG 15. Inhibition of the integrated stress response impedes UL148-mediated ER**
1019 **remodeling.** "Tet-on" ARPE-19 epithelial cells that inducibly express either UL148 or
1020 Rh159 fused to green florescent protein (gfp), i148^{gfp} (**A**) and i159^{gfp} (**B**), respectively,
1021 were induced for transgene expression using 100 ng/mL doxycycline (dox) in the
1022 presence of absence of either ISRIB (200 nM) or GSK2606414 (1.1 μM) and monitored
1023 by Western blot for expression of UL148-GFP over a series of time points (h post
1024 treatment with dox, hpt). (**C-E**): Live-cell imaging of UL148-GFP and Rh159-GFP
1025 expression patterns in the presence of ISRIB (200 nM), GSK2606414 (1.1 μM), or
1026 DMSO vehicle alone. Main scale bar represents 50 μm. For inset panels at upper left of
1027 each image, which are magnified 2.4× relative to the main image, the scale bar
1028 represents 10 μm. Also see SI Movies S8-S10.

1029

1030

1031 **FIG 16. Inhibition of the ISR prevents the coalescence of Hrd1 and UL148 into**
1032 **discrete structures during infection.** (**A**) Representative 3D maximum intensity
1033 projections of confocal imaging Z-stacks obtained from cells infected at MOI 1 for 96 h
1034 with HCMV strain TB40/E carrying an HA-tagged *UL148*, TB_148^{HA}, and maintained in
1035 the presence of ISRIB (200 nM), GSK2606414 (1.1 μM), or DMSO carrier alone (0.1%
1036 vol/vol). In merged images HA signal is shown in magenta, Hrd1 in green, and DAPI
1037 counterstaining in blue. (**B**) The percent of Hrd1 antibody signal involved in discrete
1038 structures at 96 hpi were calculated for a minimum of 30 cells per condition were
1039 determined using Imaris x64 9.3.0 software. Statistical significance was determined using
1040 a one-way ANOVA followed by Tukey's post-test; **** represents a P-value of <0.0001.
1041 The arithmetic mean for co-localization analysis results are shown as blue lines with data
1042 points for individual cells analyzed plotted as circles. (**C-D**) Western blot analyses of
1043 fibroblasts infected at MOI 1 with TB_148^{HA} and maintained in the presence of ISRIB (200
1044 nM), GSK2606414 (1.1 μM), or DMSO carrier alone (0.1%); hpi: h post infection (hpi).
1045 Note: a phospho-specific antibody was used for detection of eIF2α phosphorylated at
1046 Ser51 (P-eIF2α).
1047
1048 **SI FIGURES and MOVIES.**
1049
1050 **FIG S1**: **Additional indirect immunofluorescent confocal microscopy results from**
1051 **infected cells.** (**A**) Lower magnification overview of results from FIGS 1A-B; staining of
1052 HCMV glycoprotein H (gH) and Hrd1 at 96 h postinfection (hpi) of human fibroblasts
1053 with wildtype HCMV strain TB40/E (WT) versus *UL148*-null derivative TB_148$_{STOP}$. (**B**)

1054 Staining of gH and Hrd1 at 96 hpi of human fibroblasts with wildtype Merlin recovered
1055 from BAC-cloned Merlin pAL1393 (ME_WT) or a *UL148*-null derivative of the same
1056 virus (ME_148$_{STOP}$.) (**C**): Staining of gH and Hrd1 at 96 hpi of human fibroblasts with
1057 wildtype HCMV strain TRgfp recovered from BAC-cloned TRgfp (TR_WT) or a *UL148*-
1058 null derivative of the same virus (TR_148$_{STOP}$). (**D**) Staining of the viral tegument protein
1059 UL71 and calnexin at 5 days postinfection of human fibroblasts with primary clinical
1060 HCMV isolates obtained from patient throat swabs. (**E**) Staining against HA and Hrd1 in
1061 THP-1 macrophages fixed at 96 hpi with HCMV strain TB40/E derivative viruses
1062 TB_148^{HA} or TB_159^{HA}; note: THP-1 monocytes were differentiated using phorbol ester
1063 treatment. (**F**) Staining of HA and Hrd1 in ARPE-19 epithelial cells infected for 96 h with
1064 either TB_148^{HA} or TB_159^{HA}. (**G**) Staining of HA and Hrd1 in ARPE-19 epithelial cells
1065 infected for 96 h with HCMV strain AD169 repaired for *UL131* and to which an HA-
1066 tagged UL148 CDS from TB40/E was restored to the native *UL148* locus (AD^{r131}_148^{HA})
1067 or with a parental AD169 virus repaired for *UL131* to which *UL148* was not restored
1068 (AD^{r131}). Notes: (i) a functional *UL131* is required for efficient infection of epithelial cells;
1069 (ii) the difference in scale bar is because with ADr131 we did not employ a viral marker
1070 (e.g., HA) to identify infected cells, so the appearance of syncytia and the characteristic
1071 kidney-bean shaped nucleus was used to indicate infected cells and a slightly lower
1072 magnification was used to best show these features. (**H**) Staining for HA and Hrd1 in
1073 telomerase-immortalized rhesus fibroblasts infected with BAC-derived rhesus CMV
1074 (RhCMV) strain 68-1 carrying an HA-tag at the C-terminus of Rh159.
1075

1076 **FIG S2: Confocal microscopy of LC3B, syntaxin-6 and glycoprotein H staining**
1077 **during HCMV infection.** Human fibroblasts were infected with the indicated viruses for
1078 96 h and then fixed, permeabilized, and stained using antibodies specific for the
1079 indicated proteins. Indirect immunofluorescence images were captured using a 63X
1080 objective on a Leica SP5 confocal microscope. gH: glycoprotein H, STX6: syntaxin-6.
1081
1082 **Movie S1: STEM tomography of anomalous ER structures in wildtype HCMV**
1083 **infected fibroblasts at day 5 postinfection.**
1084
1085 **Movies S2 – S7: Live cell imaging of GFP signal following dox induction of**
1086 **transgene expression in i148^{gfp} and i159^{gfp} ARPE-19 epithelial cells:**
1087 **Movie S2: i148^{gfp} cells from 2-19 h post dox induction.**
1088 **Movie S3: i159^{gfp} cells from 2-19 h post dox induction.**
1089 **Movie S4**: **FRAP of UL148-GFP structure (ER within structure)**
1090 **Movie S5: FRAP of UL148 GFP structure (ER outside structure)**
1091 **Movie S6: FRAP of Rh159-GFP.**
1092
1093 **Movie S7: Imaging of UL148-GFP following washout of doxycycline.** (to 21 h 37
1094 min post washout).
1095 **Movie S8: i148^{gfp} cells in the presence of 0.1% DMSO, from 2-19 h post dox**
1096 **induction.**
1097 **Movie S9: i148^{gfp} cells in the presence of 1.1 μM GSK2606414, from 2-19 h post**
1098 **dox induction.**

1099 **Movie S10: i148^{gfp} cells in the presence of 200 nM ISRIB, from 2-19 h post dox**

1100 **induction.**

1101

1102

1103 **LITERATURE CITED**

1104

1105 1. Li G, Nguyen CC, Ryckman BJ, Britt WJ, Kamil JP. 2015. A viral regulator of glycoprotein
1106 complexes contributes to human cytomegalovirus cell tropism. Proc Natl Acad Sci U S A
1107 112:4471-6.
1108 2. Wille PT, Knoche AJ, Nelson JA, Jarvis MA, Johnson DC. 2010. A human cytomegalovirus
1109 gO-null mutant fails to incorporate gH/gL into the virion envelope and is unable to enter
1110 fibroblasts and epithelial and endothelial cells. J Virol 84:2585-96.
1111 3. Jiang XJ, Adler B, Sampaio KL, Digel M, Jahn G, Ettischer N, Stierhof YD, Scrivano L,
1112 Koszinowski U, Mach M, Sinzger C. 2008. UL74 of human cytomegalovirus contributes to
1113 virus release by promoting secondary envelopment of virions. J Virol 82:2802-12.
1114 4. Zhou M, Lanchy JM, Ryckman BJ. 2015. Human Cytomegalovirus gH/gL/gO Promotes the
1115 Fusion Step of Entry into All Cell Types, whereas gH/gL/UL128-131 Broadens Virus
1116 Tropism through a Distinct Mechanism. J Virol 89:8999-9009.
1117 5. Wu Y, Prager A, Boos S, Resch M, Brizic I, Mach M, Wildner S, Scrivano L, Adler B. 2017.
1118 Human cytomegalovirus glycoprotein complex gH/gL/gO uses PDGFR-alpha as a key for
1119 entry. PLoS Pathog 13:e1006281.
1120 6. Kabanova A, Marcandalli J, Zhou T, Bianchi S, Baxa U, Tsybovsky Y, Lilleri D, Silacci-Fregni
1121 C, Foglierini M, Fernandez-Rodriguez BM, Druz A, Zhang B, Geiger R, Pagani M, Sallusto
1122 F, Kwong PD, Corti D, Lanzavecchia A, Perez L. 2016. Platelet-derived growth factor-
1123 alpha receptor is the cellular receptor for human cytomegalovirus gHgLgO trimer. Nat
1124 Microbiol 1:16082.
1125 7. Wu K, Oberstein A, Wang W, Shenk T. 2018. Role of PDGF receptor-alpha during human
1126 cytomegalovirus entry into fibroblasts. Proc Natl Acad Sci U S A
1127 doi:10.1073/pnas.1806305115.
1128 8. Nguyen CC, Siddiquey MNA, Zhang H, Li G, Kamil JP. 2018. Human Cytomegalovirus
1129 Tropism Modulator UL148 Interacts with SEL1L, a Cellular Factor That Governs
1130 Endoplasmic Reticulum-Associated Degradation of the Viral Envelope Glycoprotein gO. J
1131 Virol 92:e00688-18.
1132 9. Wang ECY, Pjechova M, Nightingale K, Vlahava VM, Patel M, Ruckova E, Forbes SK,
1133 Nobre L, Antrobus R, Roberts D, Fielding CA, Seirafian S, Davies J, Murrell I, Lau B, Wilkie
1134 GS, Suarez NM, Stanton RJ, Vojtesek B, Davison A, Lehner PJ, Weekes MP, Wilkinson
1135 GWG, Tomasec P. 2018. Suppression of costimulation by human cytomegalovirus
1136 promotes evasion of cellular immune defenses. Proc Natl Acad Sci U S A 115:4998-5003.
1137 10. Siddiquey MNA, Zhang H, Nguyen CC, Domma AJ, Kamil JP. 2018. The Human
1138 Cytomegalovirus Endoplasmic Reticulum-Resident Glycoprotein UL148 Activates the
1139 Unfolded Protein Response. J Virol 92:e00896-18.
1140 11. Das S, Vasanji A, Pellett PE. 2007. Three-dimensional structure of the human
1141 cytomegalovirus cytoplasmic virion assembly complex includes a reoriented secretory
1142 apparatus. J Virol 81:11861-9.
1143 12. Sanchez V, Greis KD, Sztul E, Britt WJ. 2000. Accumulation of virion tegument and
1144 envelope proteins in a stable cytoplasmic compartment during human cytomegalovirus
1145 replication: characterization of a potential site of virus assembly. J Virol 74:975-86.

1146 13. Lilley BN, Ploegh HL. 2005. Multiprotein complexes that link dislocation, ubiquitination,
1147 and extraction of misfolded proteins from the endoplasmic reticulum membrane. Proc
1148 Natl Acad Sci U S A 102:14296-301.
1149 14. Kamhi-Nesher S, Shenkman M, Tolchinsky S, Fromm SV, Ehrlich R, Lederkremer GZ.
1150 2001. A novel quality control compartment derived from the endoplasmic reticulum.
1151 Mol Biol Cell 12:1711-23.
1152 15. Leitman J, Shenkman M, Gofman Y, Shtern NO, Ben-Tal N, Hendershot LM, Lederkremer
1153 GZ. 2014. Herp coordinates compartmentalization and recruitment of HRD1 and
1154 misfolded proteins for ERAD. Mol Biol Cell 25:1050-60.
1155 16. Houck SA, Ren HY, Madden VJ, Bonner JN, Conlin MP, Janovick JA, Conn PM, Cyr DM.
1156 2014. Quality control autophagy degrades soluble ERAD-resistant conformers of the
1157 misfolded membrane protein GnRHR. Mol Cell 54:166-179.
1158 17. Sturgill ER, Malouli D, Hansen SG, Burwitz BJ, Seo S, Schneider CL, Womack JL, Verweij
1159 MC, Ventura AB, Bhusari A, Jeffries KM, Legasse AW, Axthelm MK, Hudson AW, Sacha
1160 JB, Picker LJ, Fruh K. 2016. Natural Killer Cell Evasion Is Essential for Infection by Rhesus
1161 Cytomegalovirus. PLoS Pathog 12:e1005868.
1162 18. Chaumorcel M, Souquere S, Pierron G, Codogno P, Esclatine A. 2008. Human
1163 cytomegalovirus controls a new autophagy-dependent cellular antiviral defense
1164 mechanism. Autophagy 4:46-53.
1165 19. Chaumorcel M, Lussignol M, Mouna L, Cavignac Y, Fahie K, Cotte-Laffitte J, Geballe A,
1166 Brune W, Beau I, Codogno P, Esclatine A. 2012. The human cytomegalovirus protein
1167 TRS1 inhibits autophagy via its interaction with Beclin 1. J Virol 86:2571-84.
1168 20. Alwine JC. 2012. The human cytomegalovirus assembly compartment: a masterpiece of
1169 viral manipulation of cellular processes that facilitates assembly and egress. PLoS Pathog
1170 8:e1002878.
1171 21. Das S, Pellett PE. 2011. Spatial relationships between markers for secretory and
1172 endosomal machinery in human cytomegalovirus-infected cells versus those in
1173 uninfected cells. J Virol 85:5864-79.
1174 22. Leitman J, Ron E, Ogen-Shtern N, Lederkremer GZ. 2013. Compartmentalization of
1175 endoplasmic reticulum quality control and ER-associated degradation factors. DNA Cell
1176 Biol 32:2-7.
1177 23. Cox DW, Billingsley GD, Callahan JW. 1986. Aggregation of plasma Z type alpha 1-
1178 antitrypsin suggests basic defect for the deficiency. FEBS Lett 205:255-60.
1179 24. Le A, Ferrell GA, Dishon DS, Le QQ, Sifers RN. 1992. Soluble aggregates of the human PiZ
1180 alpha 1-antitrypsin variant are degraded within the endoplasmic reticulum by a
1181 mechanism sensitive to inhibitors of protein synthesis. J Biol Chem 267:1072-80.
1182 25. Lomas DA, Evans DL, Finch JT, Carrell RW. 1992. The mechanism of Z alpha 1-antitrypsin
1183 accumulation in the liver. Nature 357:605-7.
1184 26. Ordonez A, Snapp EL, Tan L, Miranda E, Marciniak SJ, Lomas DA. 2013. Endoplasmic
1185 reticulum polymers impair luminal protein mobility and sensitize to cellular stress in
1186 alpha1-antitrypsin deficiency. Hepatology 57:2049-60.
1187 27. Ekeowa UI, Freeke J, Miranda E, Gooptu B, Bush MF, Perez J, Teckman J, Robinson CV,
1188 Lomas DA. 2010. Defining the mechanism of polymerization in the serpinopathies. Proc
1189 Natl Acad Sci U S A 107:17146-51.

1190 28. Suhy DA, Giddings TH, Jr., Kirkegaard K. 2000. Remodeling the endoplasmic reticulum by
1191 poliovirus infection and by individual viral proteins: an autophagy-like origin for virus-
1192 induced vesicles. J Virol 74:8953-65.
1193 29. Windsor M, Hawes P, Monaghan P, Snapp E, Salas ML, Rodriguez JM, Wileman T. 2012.
1194 Mechanism of collapse of endoplasmic reticulum cisternae during African swine fever
1195 virus infection. Traffic 13:30-42.
1196 30. Miller S, Krijnse-Locker J. 2008. Modification of intracellular membrane structures for
1197 virus replication. Nat Rev Microbiol 6:363-74.
1198 31. Siddiquey MNA, Zhang H, Nguyen CC, Domma AJ, Kamil JP. 2018. The human
1199 cytomegalovirus ER resident glycoprotein UL148 activates the unfolded protein
1200 response. J Virol doi:10.1128/JVI.00896-18.
1201 32. Cormack BP, Valdivia RH, Falkow S. 1996. FACS-optimized mutants of the green
1202 fluorescent protein (GFP). Gene 173:33-8.
1203 33. Khaminets A, Heinrich T, Mari M, Grumati P, Huebner AK, Akutsu M, Liebmann L, Stolz
1204 A, Nietzsche S, Koch N, Mauthe M, Katona I, Qualmann B, Weis J, Reggiori F, Kurth I,
1205 Hubner CA, Dikic I. 2015. Regulation of endoplasmic reticulum turnover by selective
1206 autophagy. Nature 522:354-8.
1207 34. Meng L, Mohan R, Kwok BH, Elofsson M, Sin N, Crews CM. 1999. Epoxomicin, a potent
1208 and selective proteasome inhibitor, exhibits in vivo antiinflammatory activity. Proc Natl
1209 Acad Sci U S A 96:10403-8.
1210 35. Muroi M, Shiragami N, Nagao K, Yamasaki M, Takatsuki A. 1993. Folimycin
1211 (concanamycin A), a specific inhibitor of V-ATPase, blocks intracellular translocation of
1212 the glycoprotein of vesicular stomatitis virus before arrival to the Golgi apparatus. Cell
1213 Struct Funct 18:139-49.
1214 36. Muroi M, Takasu A, Yamasaki M, Takatsuki A. 1993. Folimycin (concanamycin A), an
1215 inhibitor of V-type H(+)-ATPase, blocks cell-surface expression of virus-envelope
1216 glycoproteins. Biochem Biophys Res Commun 193:999-1005.
1217 37. Kondratyev M, Avezov E, Shenkman M, Groisman B, Lederkremer GZ. 2007. PERK-
1218 dependent compartmentalization of ERAD and unfolded protein response machineries
1219 during ER stress. Exp Cell Res 313:3395-407.
1220 38. Harding HP, Novoa I, Zhang Y, Zeng H, Wek R, Schapira M, Ron D. 2000. Regulated
1221 translation initiation controls stress-induced gene expression in mammalian cells. Mol
1222 Cell 6:1099-108.
1223 39. Palam LR, Baird TD, Wek RC. 2011. Phosphorylation of eIF2 facilitates ribosomal bypass
1224 of an inhibitory upstream ORF to enhance CHOP translation. J Biol Chem 286:10939-49.
1225 40. Vattem KM, Wek RC. 2004. Reinitiation involving upstream ORFs regulates ATF4 mRNA
1226 translation in mammalian cells. Proc Natl Acad Sci U S A 101:11269-74.
1227 41. Sidrauski C, Acosta-Alvear D, Khoutorsky A, Vedantham P, Hearn BR, Li H, Gamache K,
1228 Gallagher CM, Ang KK, Wilson C, Okreglak V, Ashkenazi A, Hann B, Nader K, Arkin MR,
1229 Renslo AR, Sonenberg N, Walter P. 2013. Pharmacological brake-release of mRNA
1230 translation enhances cognitive memory. Elife 2:e00498.
1231 42. Sidrauski C, McGeachy AM, Ingolia NT, Walter P. 2015. The small molecule ISRIB
1232 reverses the effects of eIF2alpha phosphorylation on translation and stress granule
1233 assembly. Elife 4.

1234 43. Zyryanova AF, Weis F, Faille A, Alard AA, Crespillo-Casado A, Sekine Y, Harding HP, Allen
1235 F, Parts L, Fromont C, Fischer PM, Warren AJ, Ron D. 2018. Binding of ISRIB reveals a
1236 regulatory site in the nucleotide exchange factor eIF2B. Science 359:1533-1536.
1237 44. Sidrauski C, Tsai JC, Kampmann M, Hearn BR, Vedantham P, Jaishankar P, Sokabe M,
1238 Mendez AS, Newton BW, Tang EL, Verschueren E, Johnson JR, Krogan NJ, Fraser CS,
1239 Weissman JS, Renslo AR, Walter P. 2015. Pharmacological dimerization and activation of
1240 the exchange factor eIF2B antagonizes the integrated stress response. Elife 4:e07314.
1241 45. Tsai JC, Miller-Vedam LE, Anand AA, Jaishankar P, Nguyen HC, Renslo AR, Frost A, Walter
1242 P. 2018. Structure of the nucleotide exchange factor eIF2B reveals mechanism of
1243 memory-enhancing molecule. Science 359.
1244 46. Gordiyenko Y, Schmidt C, Jennings MD, Matak-Vinkovic D, Pavitt GD, Robinson CV. 2014.
1245 eIF2B is a decameric guanine nucleotide exchange factor with a gamma2epsilon2
1246 tetrameric core. Nat Commun 5:3902.
1247 47. Harding HP, Zhang Y, Ron D. 1999. Protein translation and folding are coupled by an
1248 endoplasmic-reticulum-resident kinase. Nature 397:271-4.
1249 48. Harding HP, Zhang Y, Bertolotti A, Zeng H, Ron D. 2000. Perk is essential for translational
1250 regulation and cell survival during the unfolded protein response. Mol Cell 5:897-904.
1251 49. Axten JM, Medina JR, Feng Y, Shu A, Romeril SP, Grant SW, Li WH, Heerding DA,
1252 Minthorn E, Mencken T, Atkins C, Liu Q, Rabindran S, Kumar R, Hong X, Goetz A, Stanley
1253 T, Taylor JD, Sigethy SD, Tomberlin GH, Hassell AM, Kahler KM, Shewchuk LM, Gampe
1254 RT. 2012. Discovery of 7-methyl-5-(1-{[3-(trifluoromethyl)phenyl]acetyl}-2,3-dihydro-1H-
1255 indol-5-yl)-7H-p yrrolo[2,3-d]pyrimidin-4-amine (GSK2606414), a potent and selective
1256 first-in-class inhibitor of protein kinase R (PKR)-like endoplasmic reticulum kinase
1257 (PERK). J Med Chem 55:7193-207.
1258 50. Tenorio R, Fernandez de Castro I, Knowlton JJ, Zamora PF, Lee CH, Mainou BA, Dermody
1259 TS, Risco C. 2018. Reovirus sigmaNS and muNS Proteins Remodel the Endoplasmic
1260 Reticulum to Build Replication Neo-Organelles. MBio 9.
1261 51. Miller S, Kastner S, Krijnse-Locker J, Buhler S, Bartenschlager R. 2007. The non-structural
1262 protein 4A of dengue virus is an integral membrane protein inducing membrane
1263 alterations in a 2K-regulated manner. J Biol Chem 282:8873-82.
1264 52. Lamond AI, Sleeman JE. 2003. Nuclear substructure and dynamics. Curr Biol 13:R825-8.
1265 53. Granell S, Baldini G, Mohammad S, Nicolin V, Narducci P, Storrie B, Baldini G. 2008.
1266 Sequestration of mutated alpha1-antitrypsin into inclusion bodies is a cell-protective
1267 mechanism to maintain endoplasmic reticulum function. Mol Biol Cell 19:572-86.
1268 54. Lawless MW, Greene CM, Mulgrew A, Taggart CC, O'Neill SJ, McElvaney NG. 2004.
1269 Activation of endoplasmic reticulum-specific stress responses associated with the
1270 conformational disease Z alpha 1-antitrypsin deficiency. J Immunol 172:5722-6.
1271 55. Tirosh B, Iwakoshi NN, Lilley BN, Lee AH, Glimcher LH, Ploegh HL. 2005. Human
1272 cytomegalovirus protein US11 provokes an unfolded protein response that may
1273 facilitate the degradation of class I major histocompatibility complex products. J Virol
1274 79:2768-79.
1275 56. Wiertz EJ, Jones TR, Sun L, Bogyo M, Geuze HJ, Ploegh HL. 1996. The human
1276 cytomegalovirus US11 gene product dislocates MHC class I heavy chains from the
1277 endoplasmic reticulum to the cytosol. Cell 84:769-79.

1278 57. van den Boomen DJ, Timms RT, Grice GL, Stagg HR, Skodt K, Dougan G, Nathan JA,
1279 Lehner PJ. 2014. TMEM129 is a Derlin-1 associated ERAD E3 ligase essential for virus-
1280 induced degradation of MHC-I. Proc Natl Acad Sci U S A 111:11425-30.
1281 58. Caramelo JJ, Parodi AJ. 2008. Getting in and out from calnexin/calreticulin cycles. J Biol
1282 Chem 283:10221-5.
1283 59. Hammond C, Braakman I, Helenius A. 1994. Role of N-linked oligosaccharide
1284 recognition, glucose trimming, and calnexin in glycoprotein folding and quality control.
1285 Proc Natl Acad Sci U S A 91:913-7.
1286 60. Zhou M, Yu Q, Wechsler A, Ryckman BJ. 2013. Comparative analysis of gO isoforms
1287 reveals that strains of human cytomegalovirus differ in the ratio of gH/gL/gO and
1288 gH/gL/UL128-131 in the virion envelope. J Virol 87:9680-90.
1289 61. Zhang L, Zhou M, Stanton R, Kamil J, Ryckman BJ. 2018. Expression Levels of
1290 Glycoprotein O (gO) Vary between Strains of Human Cytomegalovirus, Influencing the
1291 Assembly of gH/gL Complexes and Virion Infectivity. J Virol 92.
1292 62. Sifers RN, Brashears-Macatee S, Kidd VJ, Muensch H, Woo SL. 1988. A frameshift
1293 mutation results in a truncated alpha 1-antitrypsin that is retained within the rough
1294 endoplasmic reticulum. J Biol Chem 263:7330-5.
1295 63. Choudhury P, Liu Y, Bick RJ, Sifers RN. 1997. Intracellular association between UDP-
1296 glucose:glycoprotein glucosyltransferase and an incompletely folded variant of alpha1-
1297 antitrypsin. J Biol Chem 272:13446-51.
1298 64. Tsao YS, Ivessa NE, Adesnik M, Sabatini DD, Kreibich G. 1992. Carboxy terminally
1299 truncated forms of ribophorin I are degraded in pre-Golgi compartments by a calcium-
1300 dependent process. J Cell Biol 116:57-67.
1301 65. de Virgilio M, Weninger H, Ivessa NE. 1998. Ubiquitination is required for the retro-
1302 translocation of a short-lived luminal endoplasmic reticulum glycoprotein to the cytosol
1303 for degradation by the proteasome. J Biol Chem 273:9734-43.
1304 66. Johnston JA, Ward CL, Kopito RR. 1998. Aggresomes: a cellular response to misfolded
1305 proteins. J Cell Biol 143:1883-98.
1306 67. Johnston JA, Illing ME, Kopito RR. 2002. Cytoplasmic dynein/dynactin mediates the
1307 assembly of aggresomes. Cell Motil Cytoskeleton 53:26-38.
1308 68. Pankiv S, Alemu EA, Brech A, Bruun JA, Lamark T, Overvatn A, Bjorkoy G, Johansen T.
1309 2010. FYCO1 is a Rab7 effector that binds to LC3 and PI3P to mediate microtubule plus
1310 end-directed vesicle transport. J Cell Biol 188:253-69.
1311 69. Hummel T, Krukkert K, Roos J, Davis G, Klambt C. 2000. Drosophila Futsch/22C10 is a
1312 MAP1B-like protein required for dendritic and axonal development. Neuron 26:357-70.
1313 70. Wang H, Bedford FK, Brandon NJ, Moss SJ, Olsen RW. 1999. GABA(A)-receptor-
1314 associated protein links GABA(A) receptors and the cytoskeleton. Nature 397:69-72.
1315 71. Li YR, King OD, Shorter J, Gitler AD. 2013. Stress granules as crucibles of ALS
1316 pathogenesis. J Cell Biol 201:361-72.
1317 72. Zhang K, Daigle JG, Cunningham KM, Coyne AN, Ruan K, Grima JC, Bowen KE, Wadhwa
1318 H, Yang P, Rigo F, Taylor JP, Gitler AD, Rothstein JD, Lloyd TE. 2018. Stress Granule
1319 Assembly Disrupts Nucleocytoplasmic Transport. Cell 173:958-971 e17.
1320 73. Hetz C, Saxena S. 2017. ER stress and the unfolded protein response in
1321 neurodegeneration. Nat Rev Neurol 13:477-491.

1322 74. Kirchoff V, Wong S, St JS, Pari GS. 2002. Generation of a life-expanded rhesus monkey
1323 fibroblast cell line for the growth of rhesus rhadinovirus (RRV). Arch Virol 147:321-33.
1324 75. Sinzger C, Hahn G, Digel M, Katona R, Sampaio KL, Messerle M, Hengel H, Koszinowski U,
1325 Brune W, Adler B. 2008. Cloning and sequencing of a highly productive, endotheliotropic
1326 virus strain derived from human cytomegalovirus TB40/E. J Gen Virol 89:359-68.
1327 76. Smith IL, Taskintuna I, Rahhal FM, Powell HC, Ai E, Mueller AJ, Spector SA, Freeman WR.
1328 1998. Clinical failure of CMV retinitis with intravitreal cidofovir is associated with
1329 antiviral resistance. Arch Ophthalmol 116:178-85.
1330 77. Murphy E, Yu D, Grimwood J, Schmutz J, Dickson M, Jarvis MA, Hahn G, Nelson JA,
1331 Myers RM, Shenk TE. 2003. Coding potential of laboratory and clinical strains of human
1332 cytomegalovirus. Proc Natl Acad Sci U S A 100:14976-81.
1333 78. Stanton RJ, Baluchova K, Dargan DJ, Cunningham C, Sheehy O, Seirafian S, McSharry BP,
1334 Neale ML, Davies JA, Tomasec P, Davison AJ, Wilkinson GW. 2010. Reconstruction of the
1335 complete human cytomegalovirus genome in a BAC reveals RL13 to be a potent inhibitor
1336 of replication. J Clin Invest 120:3191-208.
1337 79. Hobom U, Brune W, Messerle M, Hahn G, Koszinowski UH. 2000. Fast screening
1338 procedures for random transposon libraries of cloned herpesvirus genomes: mutational
1339 analysis of human cytomegalovirus envelope glycoprotein genes. J Virol 74:7720-9.
1340 80. Chang WL, Barry PA. 2003. Cloning of the full-length rhesus cytomegalovirus genome as
1341 an infectious and self-excisable bacterial artificial chromosome for analysis of viral
1342 pathogenesis. J Virol 77:5073-83.
1343 81. Tischer BK, Smith GA, Osterrieder N. 2010. En passant mutagenesis: a two step
1344 markerless red recombination system. Methods Mol Biol 634:421-30.
1345 82. Tischer BK, von Einem J, Kaufer B, Osterrieder N. 2006. Two-step red-mediated
1346 recombination for versatile high-efficiency markerless DNA manipulation in Escherichia
1347 coli. Biotechniques 40:191-7.
1348 83. Dietz AN, Villinger C, Becker S, Frick M, von Einem J. 2018. A Tyrosine-Based Trafficking
1349 Motif of the Tegument Protein pUL71 Is Crucial for Human Cytomegalovirus Secondary
1350 Envelopment. J Virol 92.
1351 84. Hohn K, Sailer M, Wang L, Lorenz M, Schneider ME, Walther P. 2011. Preparation of
1352 cryofixed cells for improved 3D ultrastructure with scanning transmission electron
1353 tomography. Histochem Cell Biol 135:1-9.
1354 85. Villinger C, Schauflinger M, Gregorius H, Kranz C, Hohn K, Nafeey S, Walther P. 2014.
1355 Three-dimensional imaging of adherent cells using FIB/SEM and STEM. Methods Mol
1356 Biol 1117:617-38.
1357 86. Kremer JR, Mastronarde DN, McIntosh JR. 1996. Computer visualization of three-
1358 dimensional image data using IMOD. J Struct Biol 116:71-6.
1359 87. Britt WJ, Jarvis MA, Drummond DD, Mach M. 2005. Antigenic domain 1 is required for
1360 oligomerization of human cytomegalovirus glycoprotein B. J Virol 79:4066-79.
1361

1362

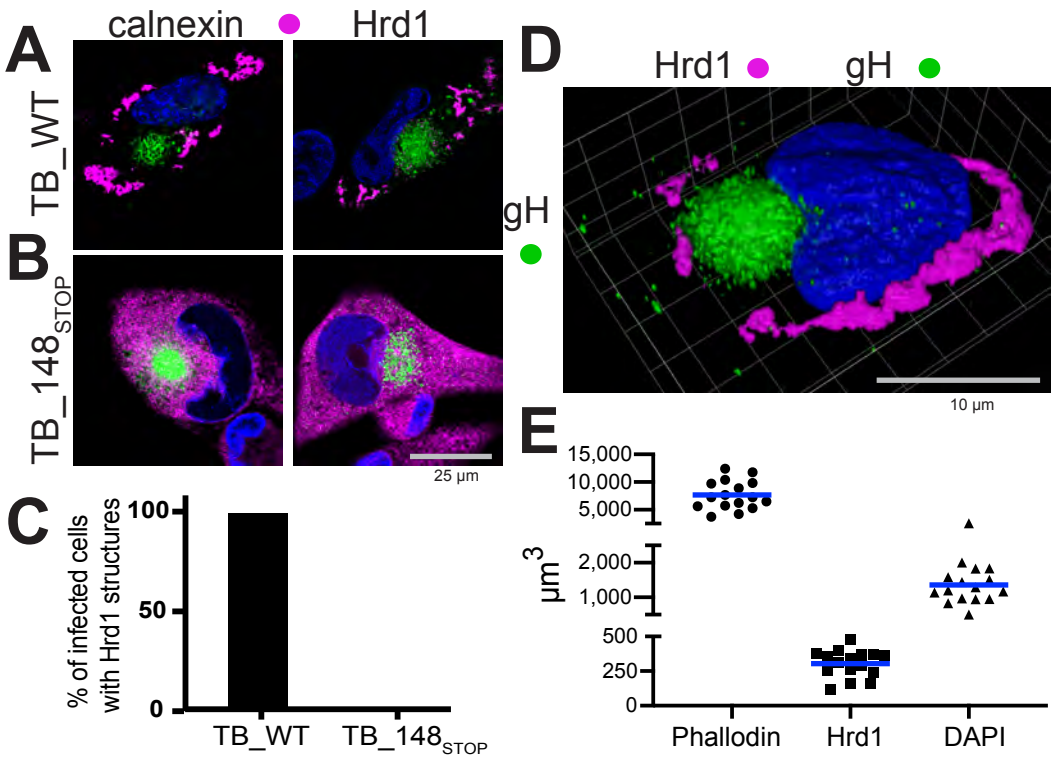

FIG 1. UL148 reorganizes ER markers into anomalous structures during HCMV infection. Fibroblasts infected at 1 MOI with either **(A)** wildtype HCMV strain TB40/E (TB_WT) or **(B)** an isogenic *UL148*-null mutant (TB_148$_{STOP}$), were fixed at 96 h postinfection (hpi) and imaged by confocal microscopy after staining with antibodies specific for calnexin or Hrd1 (magenta) and glycoprotein H (gH, green), as indicated. DAPI (blue) signal was used to counterstain nuclei. **(C)** Percentage of fibroblasts that contain Hrd1 structures at 96 hpi; fifty gH-positive cells for each condition were scored for the presence or absence of UL148 structures (also see SI Fig S1A). (**D**) Three-dimensional confocal image projection of a TB_WT infected fibroblast stained at 96 hpi for Hrd1 and gH. **(E)** Volumetric measurements were made from sixteen infected cells, stained with phalloidin-AlexaFluor 594 conjugate to estimate total cell volume, with Hrd1 antibody to estimate the volume of UL148-dependent ER structures, and with DAPI to estimate nuclear volume.

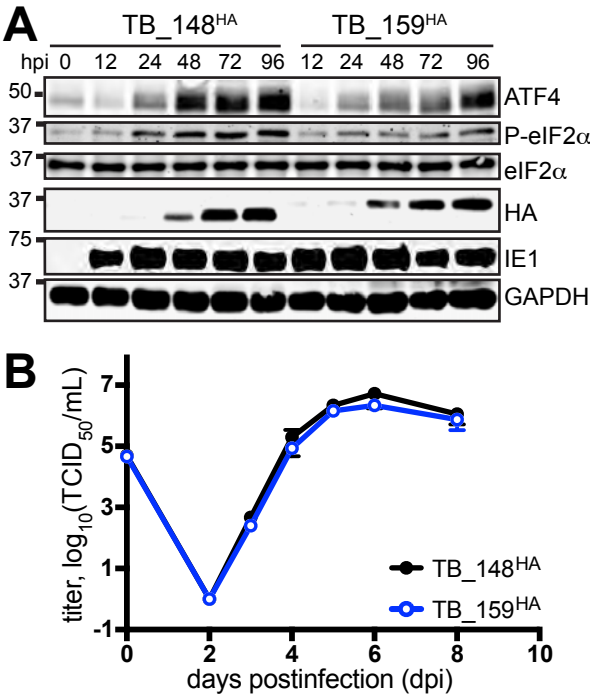

FIG 2. Characterization of TB_148^{HA} and TB_159^{HA} viruses. (A) Human fibroblasts were infected at MOI 1 with the indicated recombinant HCMVs and whole cell lysate samples harvested at the indicated times post-infection (h post-infection: hpi) were analyzed by Western blot to detect HA-tagged UL148 or Rh159, the 72 kD viral nuclear antigen IE1-72 (IE1), and GAPDH. **(B)** Single-cycle viral replication kinetic curves from MOI 1 infected fibroblasts were plotted by determining the titer in tissue culture infectious dose 50 ($TCID_{50}$) from supernatants collected at the indicated times postinfection.

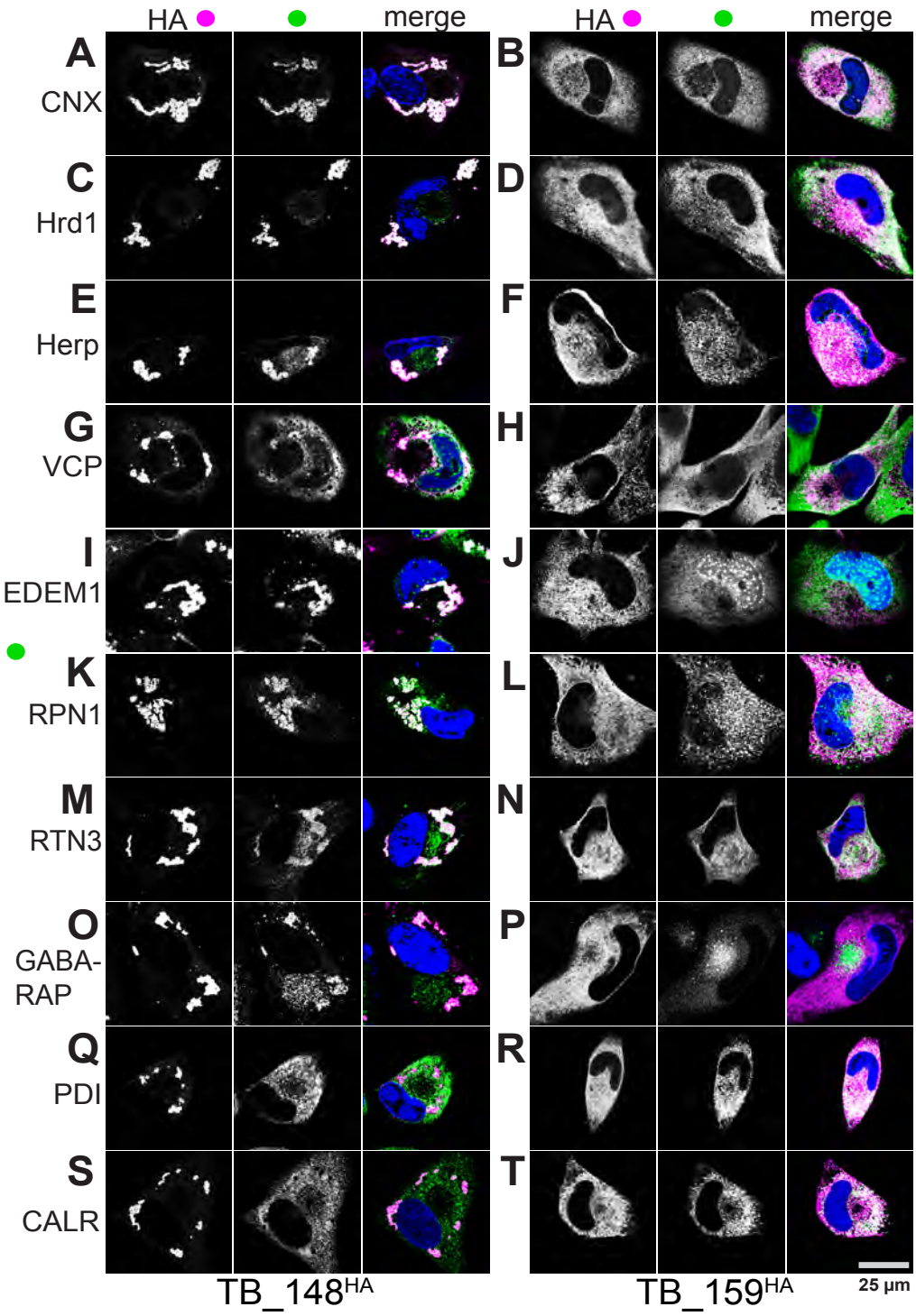

FIG 3. UL148 localizes to unusual ER compartments enriched for glycoprotein quality control markers. Fibroblasts infected at MOI 1 with either TB_148^{HA} (panels: **A, C, E, G, I, K, M, O, Q, S**) or TB_159^{HA} (panels: **B, D, F, H, J, L, N, P, R, T**) were fixed at 96 hpi, and imaged by confocal microscopy after co-staining with antibodies specific for HA (UL148/Rh159, magenta in merge) and the indicated cellular markers (green in merge). DAPI (blue) counterstaining is shown in merged image.

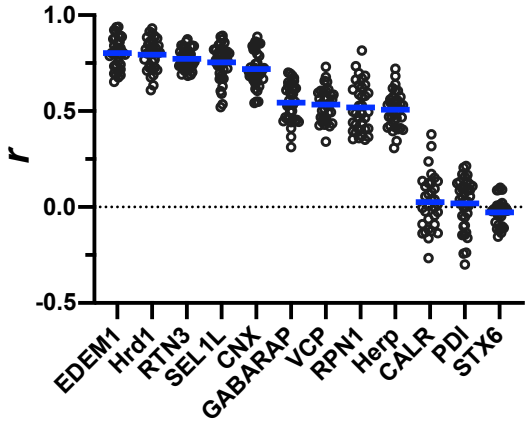

FIG 4. Quantification of Co-localization between UL148 and Cellular Markers. A Pearson's correlation coefficient (*r*) was calculated using NIH ImageJ software to estimate the degree of co-localization between UL148 (HA signal) and each of the indicated cellular markers. A minimum of 30 cells were analyzed per marker. The arithmetic mean for each co-localization analysis result is shown as a blue line, and data points for individual cells analyzed are plotted as circles.

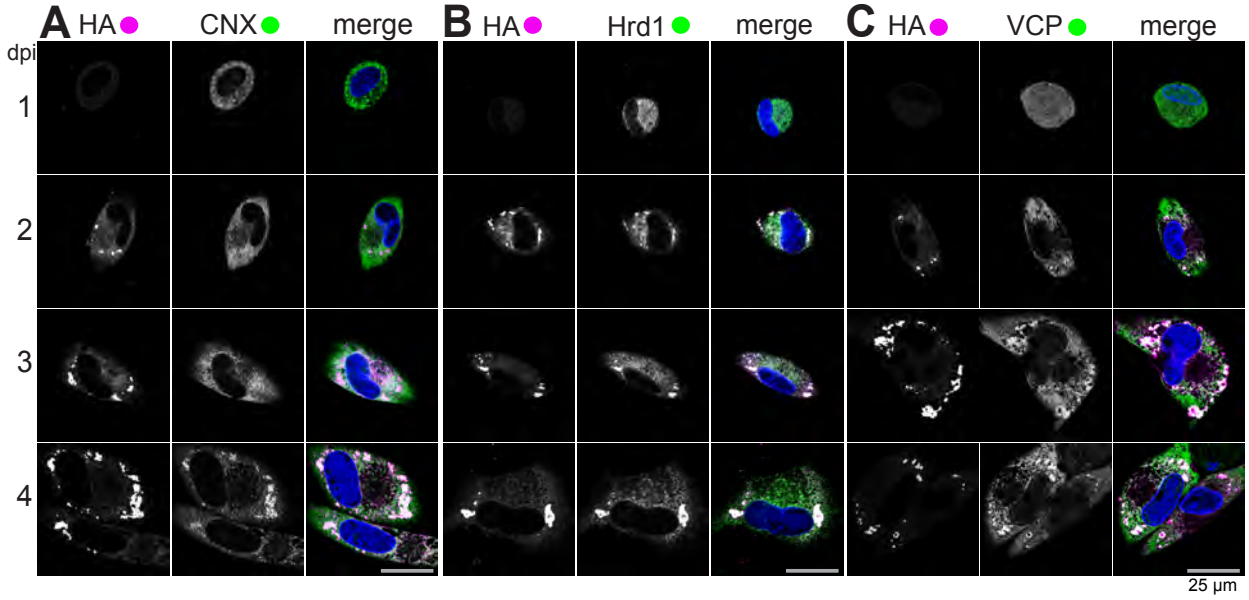

FIG 5. Cellular proteins involved in glycoprotein quality control are recruited with differing kinetics to UL148 ER structures. Fibroblasts infected with TB_148^{HA} at 1 MOI were fixed at the indicated time points (days post infection, dpi) and imaged by confocal microscopy after staining with antibodies specific for HA (UL148, magenta), CNX (green, **A**) , Hrd1 (green, **B**) or VCP(green, **C**), DAPI (blue).

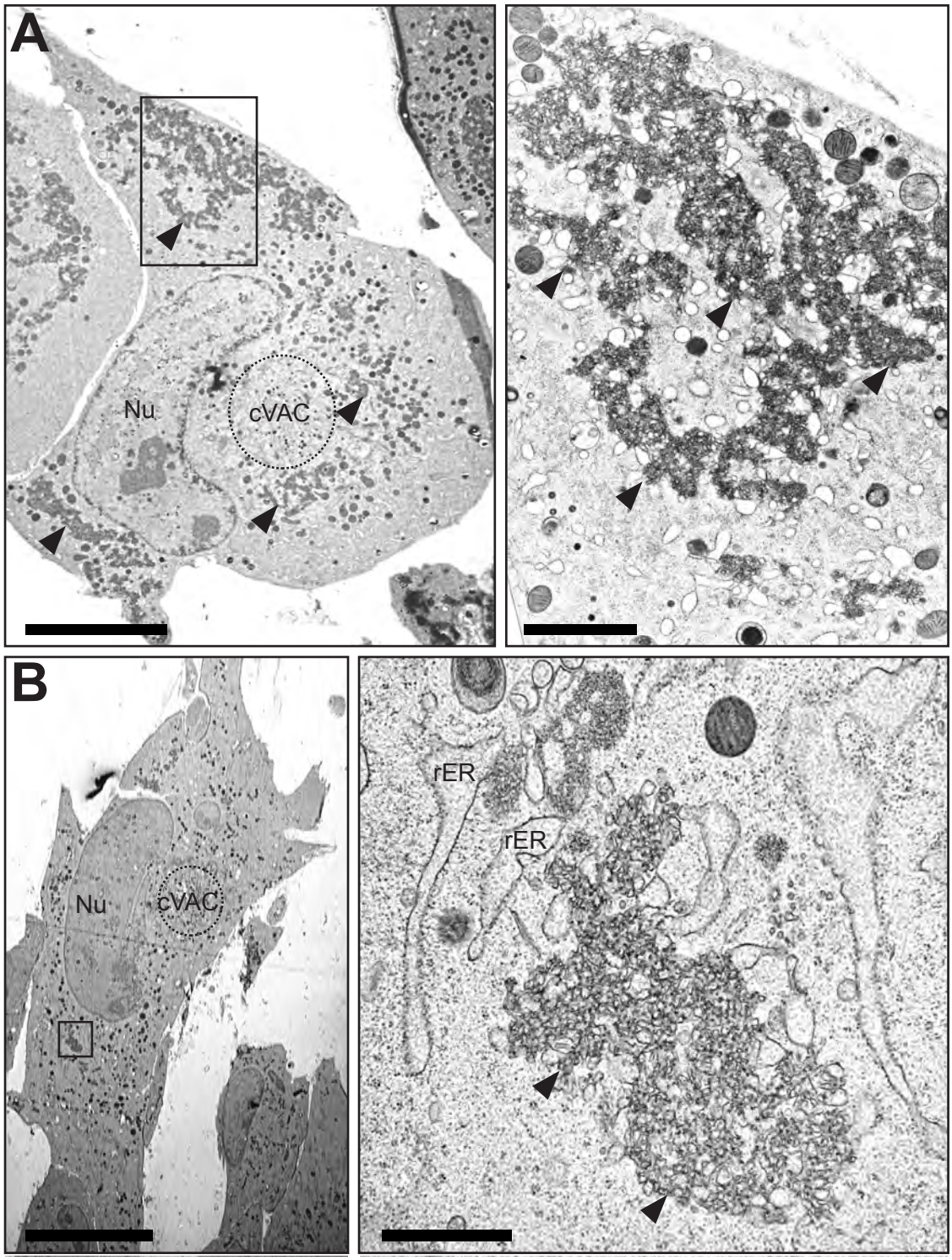

FIG 6. TEM of ER structures in wildtype HCMV infected cells. Human fibroblasts infected with wildtype HCMV (TB_WT) were fixed by high-pressure freezing and freeze substitution at day 5 postinfection and imaged using TEM. Panels (**A**) and (**B**) show cell overview at left. For each cell, the boxed region is shown at higher magnification. Scale bars; left panels: 10 µm, right panels: 2 µm. rER: rough ER; Nu: nucleus; cVAC: cytoplasmic viral assembly compartment. Solid arrowheads indicate the UL148-dependent ER structures of interest.

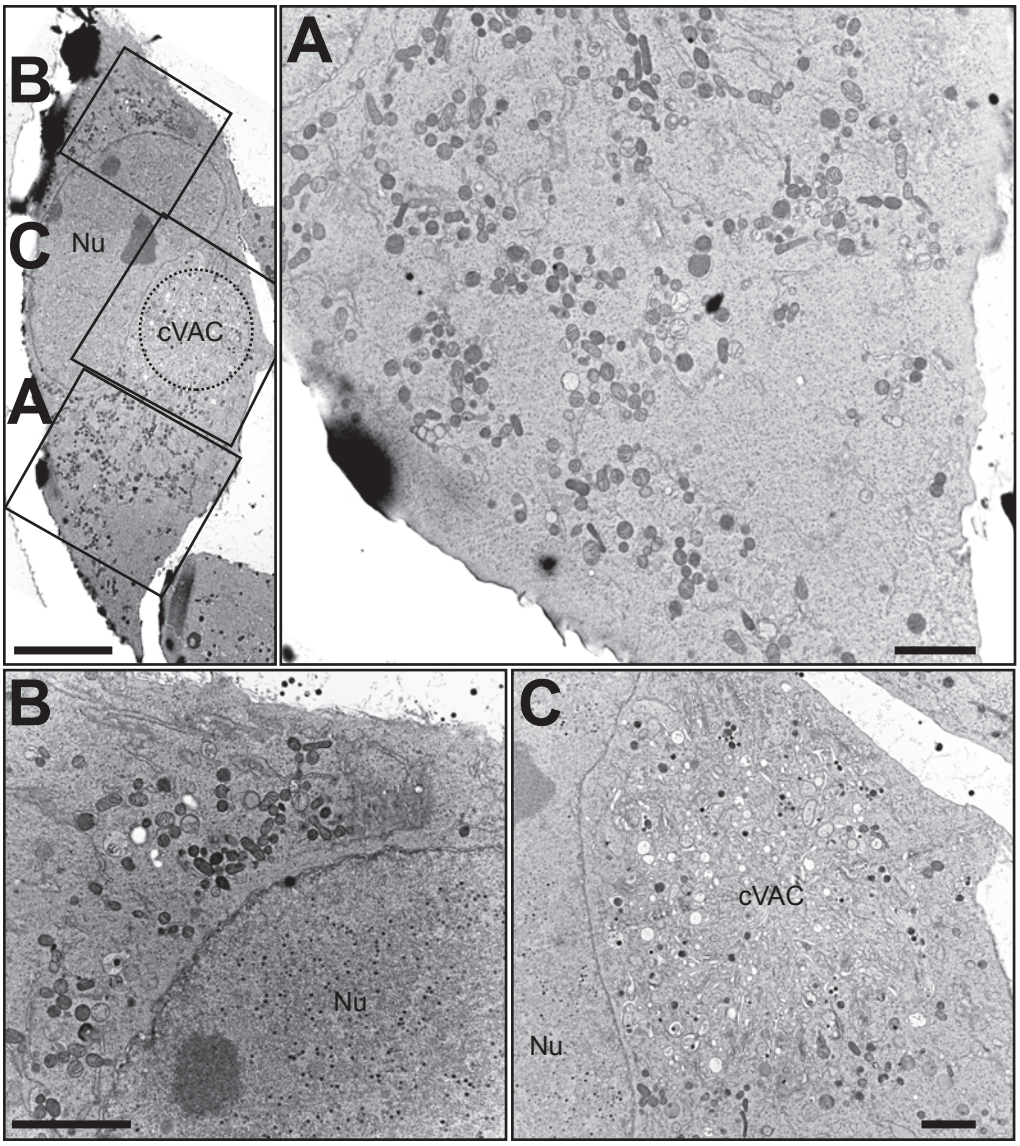

FIG 7. TEM of *UL148*-null HCMV infected cells. Human fibroblasts infected with a *UL148*-null mutant (TB_148$_{STOP}$) were fixed by high-pressure freezing and freeze substitution at day 5 postinfection and imaged using TEM. At the upper left an overview panel of a representative cell is shown with panels **A, B, and C** each boxed. The boxed regions are expanded at higher magnification at right (**A**) and below (**B, C**). Scale bars for upper left overview panel: 10 µm, for zoomed panels: 2 µm. rER: rough ER; Nu: nucleus; cVAC: cytoplasmic viral assembly compartment.

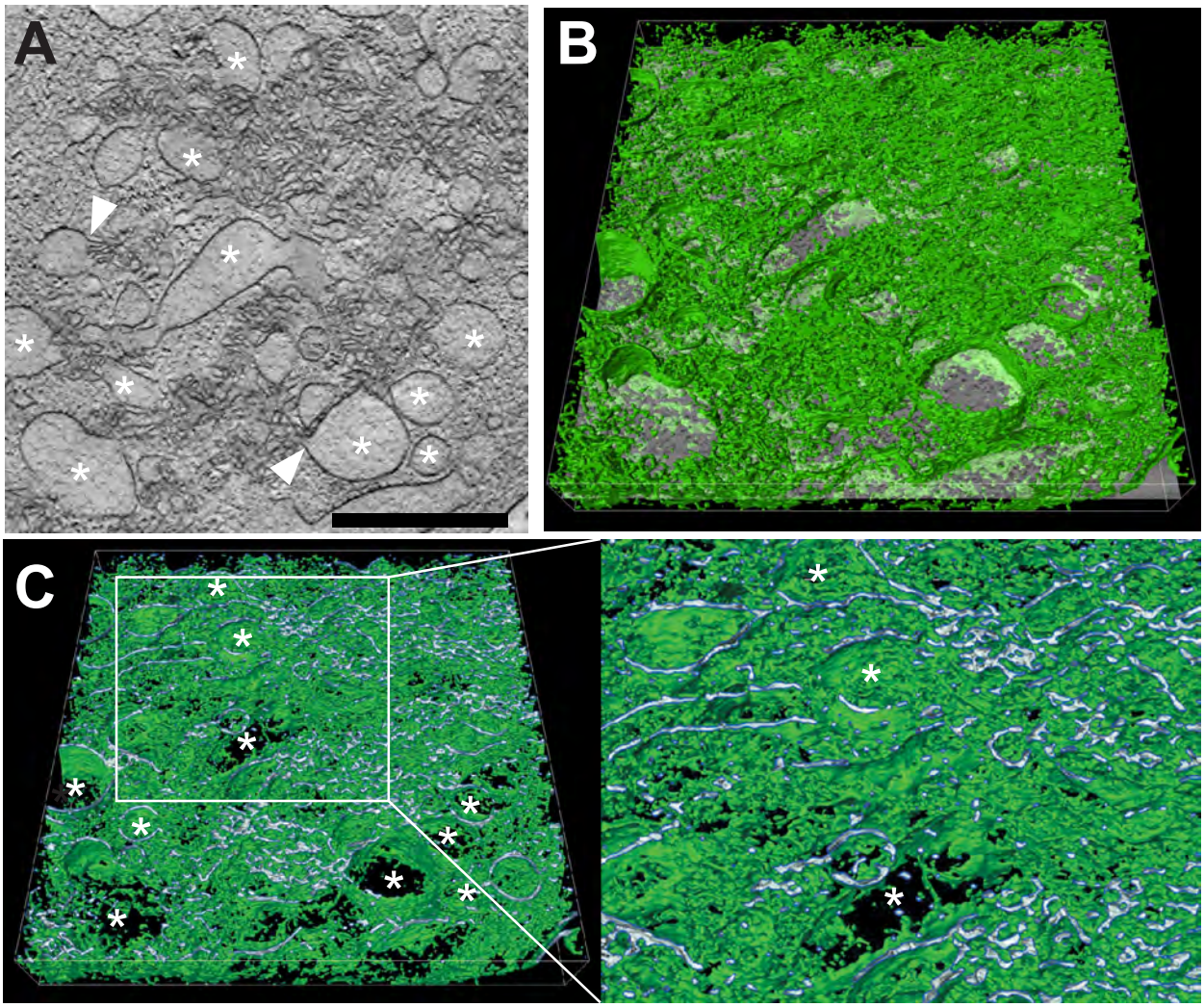

FIG 8. STEM tomography of UL148-dependent ER structures in HCMV infected cells. Human fibroblasts infected with wildtype HCMV (TB_WT) were fixed by high-pressure freezing and freeze substitution at day 5 postinfection and tomograms were recorded by STEM. (**A**) Shows a virtual section through the tomogram of a virus-induced membranous structure; asterisks denote ER structures of distended lumenal space. White arrowheads indicate sites at which membranes originating from distended ER cisternae continue into areas of involuted collapsed ER. Scale bar: 1 µm. (**B**) Shows the same virtual section as in (A) tilted and with a 3D visualization of the membranous network (green) of the entire tomogram. The same distended ER cisternae as in (A) are marked by asterisks. (**C**) Shows a cross section through (B) to visualize the membrane profile of the membranous structures. The region delimited by a white box is shown in a higher magnification on the right. Finer detail of the enlarged ER cisternae and the connections between them are readily visible; asterisks indicate the same distended ER cisternae as in (A) and (B). Also, see SI Movie S1. Scale bar: 1 µm.

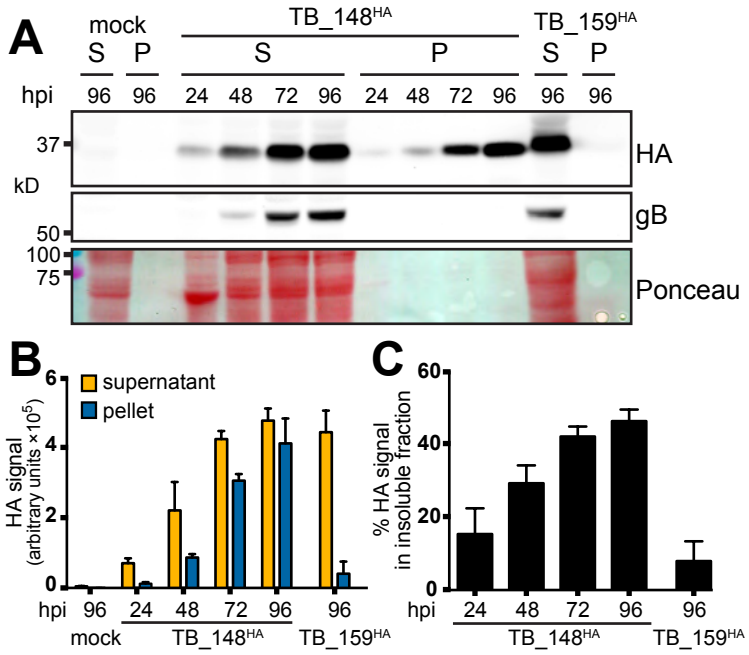

FIG 9. Solubility Analysis of UL148 and Rh159. (**A**) Human fibroblasts were infected at MOI 1 $TCID_{50}$/cell with HCMV strain TB40/E derived viruses TB_148^{HA}, which expresses UL148 fused at its C-terminus to an HA-epitope tag, or TB_159^{HA}, which lacks *UL148* and instead expresses rhesus CMV Rh159 carrying a C-terminal HA tag. At the indicated times postinfection (hpi), infected cells were collected radioimmunoprecipitation (RIPA) lysis buffer, centrifuged at 21,000×g for 30 min, after which supernatant (sup) and pellet (pel) fractions were boiled in gel loading buffer containing 2% sodium dodecyl sulfate (SDS). Equivalent portions of supernatant and pellet were resolved by SDS-polyacrylamide gel electrophoresis, transferred to a nitrocellulose membrane for detection of protein species immunoreactive to antibodies against HA epitope (HA) and HCMV glycoprotein B (gB) and for total protein signal using Ponceau S reagent (Ponceau). (**B-C**). Signal intensity of fluorophore-conjugated secondary antibodies in anti-HA Western blots were measured from three independent biological replicates of the experiment shown in (A); error bars indicate standard deviation. (**B**) The fluorescent signal for each infection time point condition (Y-axis indicates arbitrary units, in hundred thousands). (**C**) The amount of signal found in the insoluble (pellet) fraction relative to the total signal (pellet plus supernatant) for each infection time point are plotted as percentage values.

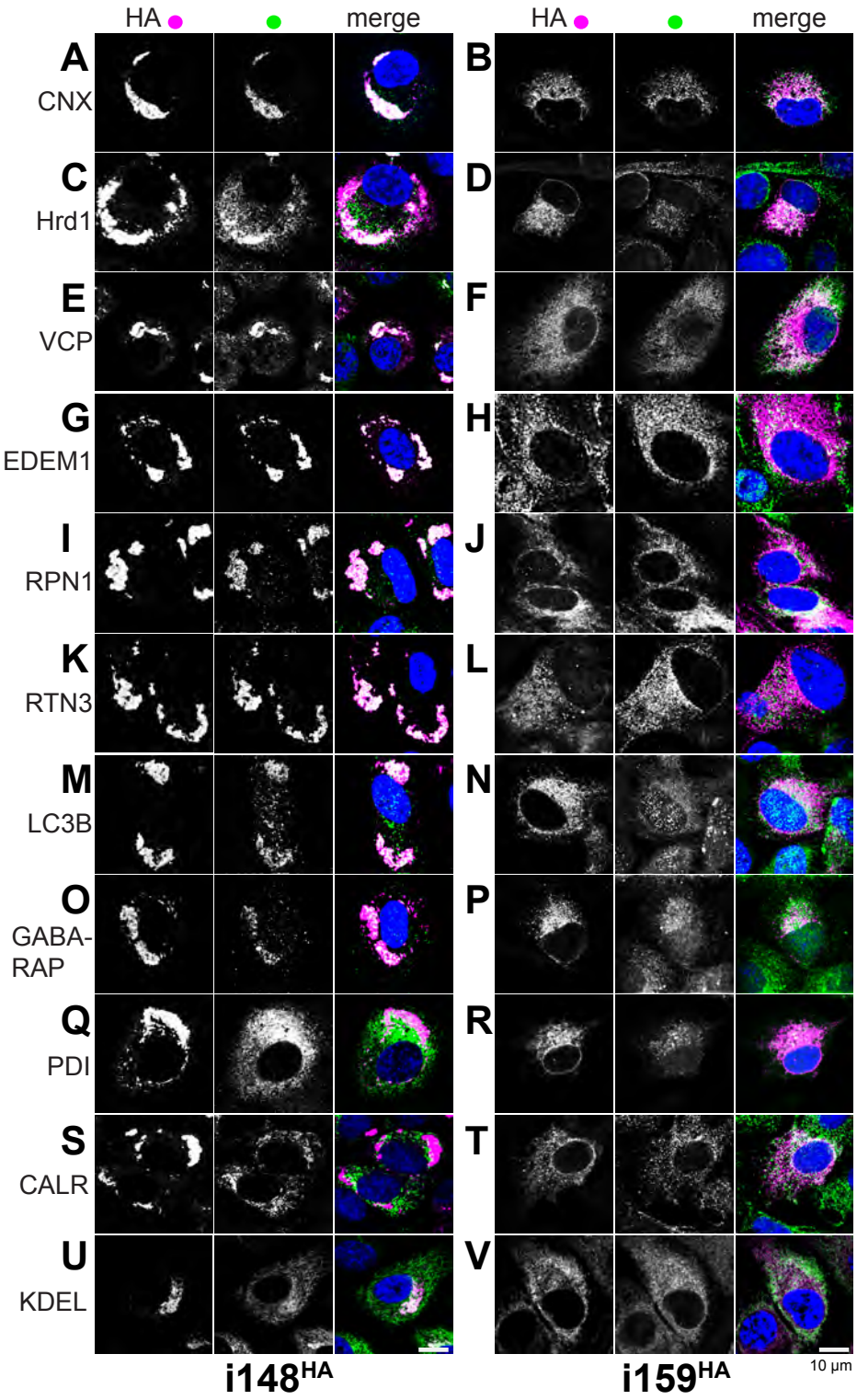

FIG 10. UL148 is sufficient to remodel the ER. HA-tagged UL148 or Rh159 were doxycycline (dox) induced in the context of a "tet-on" lentiviral vector system in stably transduced ARPE-19 epithelial cell populations, i148^{HA} and i159^{HA}, respectively. Cells were fixed at 48 h postinduction for indirect immunofluorescence staining for the indicated cellular markers (green) together with HA (magenta). Scale bar: 10 µm.

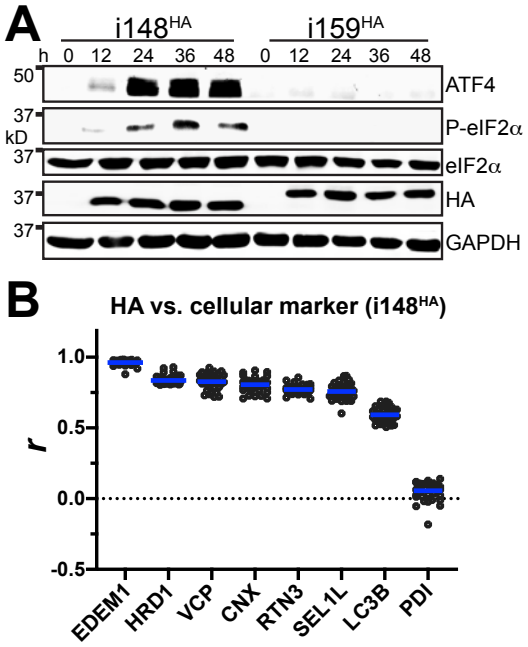

FIG 11. ISR activation accompanies redistribution of ER markers during ectopic expression of UL148. (A) Lysates of tet-on ARPE-19 cells expressing either UL148 or Rh159 fused to an HA tag, i148HA and i159HA, respectively, were collected at the indicated times post doxycycline (dox) induction and analyzed by Western blot for the expression of the indicated proteins and for the abundance of eIF2α phosphorylated at Ser51 (P-eIF2α) using a phospho-specific antibody. (**B**) Pearson's correlation coefficient (*r*) values were calculated using NIH ImageJ software estimate the degree of co-localization between UL148 (HA signal) and the indicated cellular markers. A minimum of 30 cells were analyzed per marker. Arithmetic means for each co-localization analysis result are shown as blue lines, and data points for individual cells analyzed are plotted as circles.

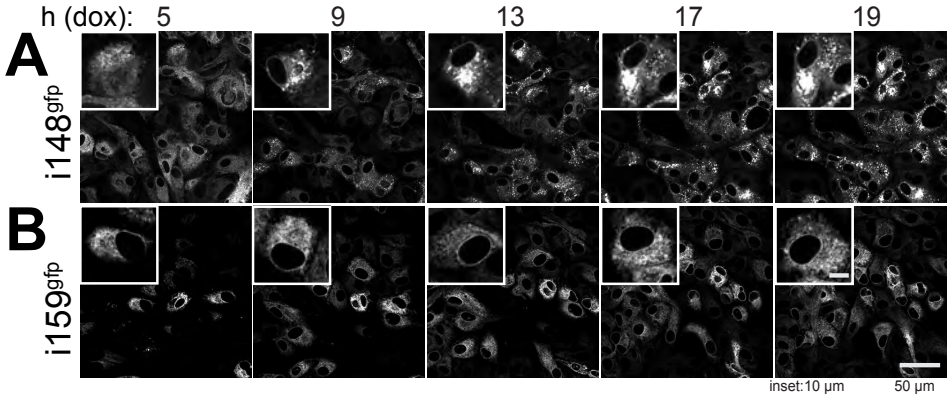

FIG 12. Live Cell Imaging of UL148-GFP and Rh159-GFP during Induced Ectopic Expression. "Tet-on" ARPE-19 epithelial cells that inducibly express either UL148 or Rh159 fused to green florescent protein (gfp), i148^{gfp} (**A**) and i159^{gfp} (**B**), respectively, were induced for transgene expression using 100 ng/mL doxycycline (dox) and imaged using live-cell microscopy. Images from the selected time points (h post treatment with dox, hpt) are shown. The main scale bar represents 50 µm. For inset panels at upper left of each image, which are magnified 2.4× relative to the main image, the scale bar represents 10 µm. Also see SI Movies S2-S3.

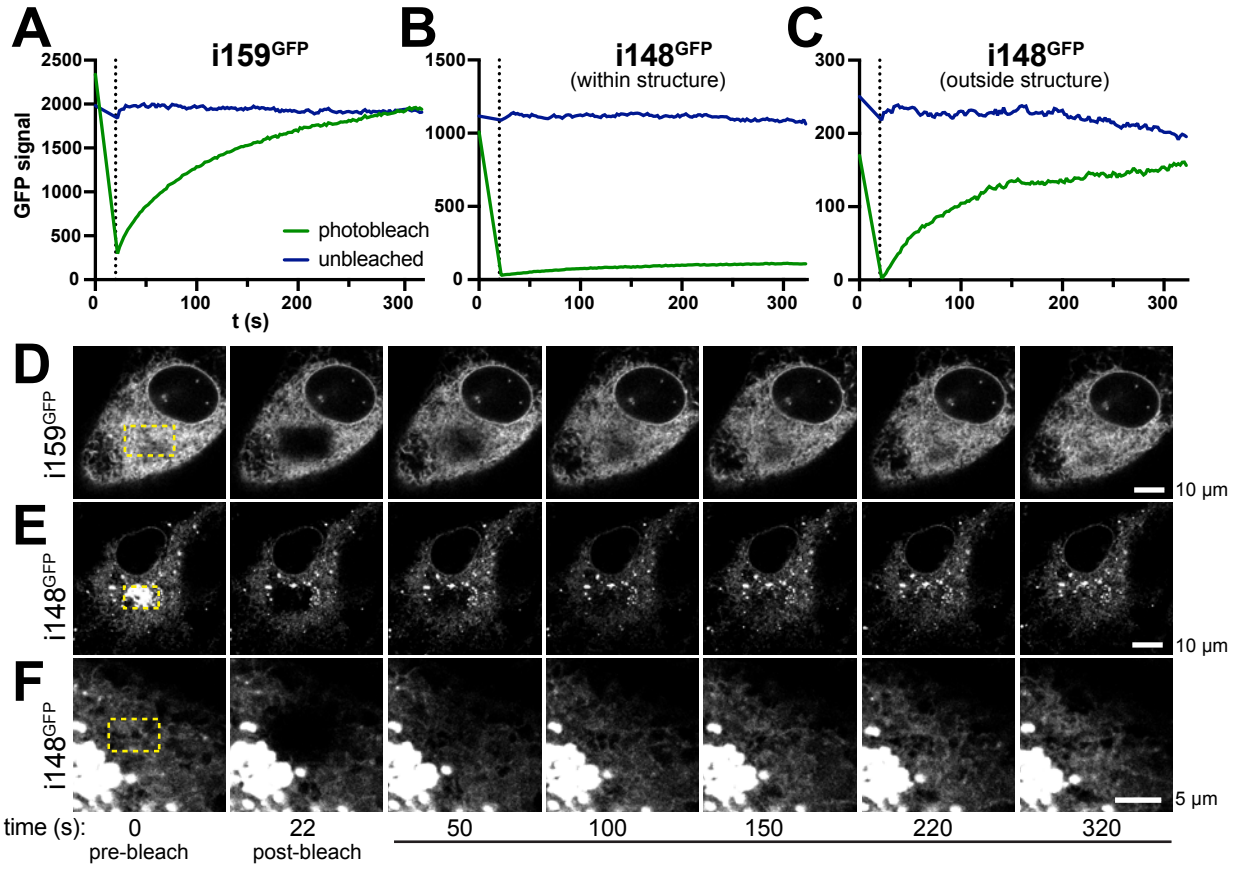

FIG 13. FRAP analysis. ARPE-19 cells that inducibly express Rh159-GFP, i159^{gfp} (**A**) or UL148-GFP, i148^{gfp} (**B-C**) were doxycycline induced for 24 h (100 ng/mL doxycycline (dox). Separate regions of GFP signal in selected cells were photobleached (405 nm laser) or left unbleached, while a third region lacking GFP signal was chosen as a background reference were measured before and during fluorescence recovery after photobleaching (FRAP). Note: background signal was not plotted because values were resolvable from the x-axis. GFP signal intensity is plotted over a time period (seconds, s) starting with an exposure at t=0 (immediately before photobleaching), and including measurements taken every 2 s after photobleaching (0-20 s) until termination of the measurement series at t=322 s (300 s of FRAP). (**D-F**) Images from the selected time points (s, seconds) immediately before and after bleaching, and during fluorescence recovery period. Also see SI Movies S4-S6.

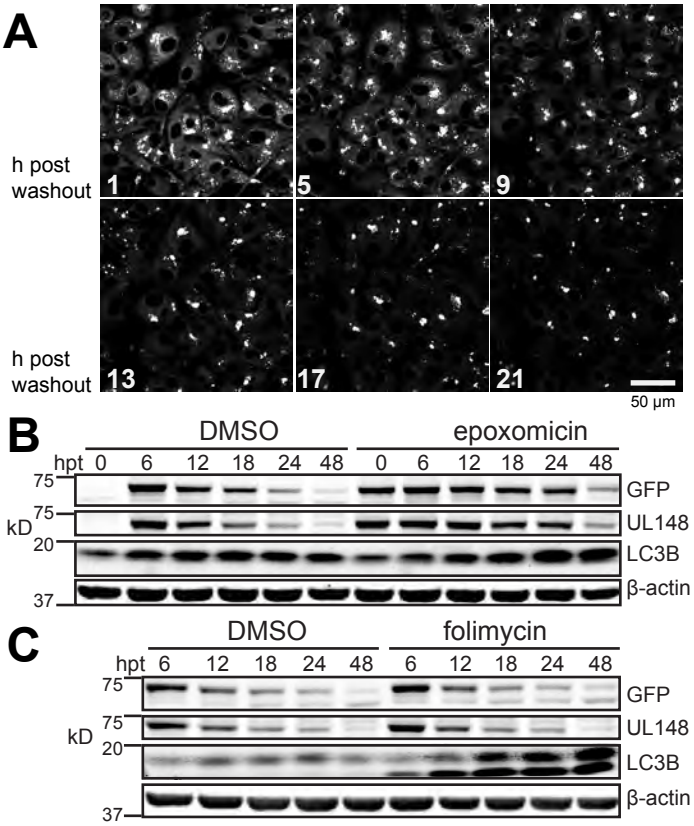

FIG 14: UL148-GFP is stabilized by inhibition of proteasomal but not lysosomal degradation. "Tet-on" ARPE-19 cells that inducibly express UL148-GFP (i148^{gfp}) were induced for 24 h by the addition of 100 ng/mL doxycycline (dox), after which the dox inducing agent was washed out and medium containing either the proteasome inhibitor epoxomicin (20 µM) or the proton pump inhibitor folimycin (115 nM) was added and samples were harvested for Western blot analysis at the indicated times post treatment (h post treatment, hpt) with folimycin or epoxomicin. Also see SI Movie S7.

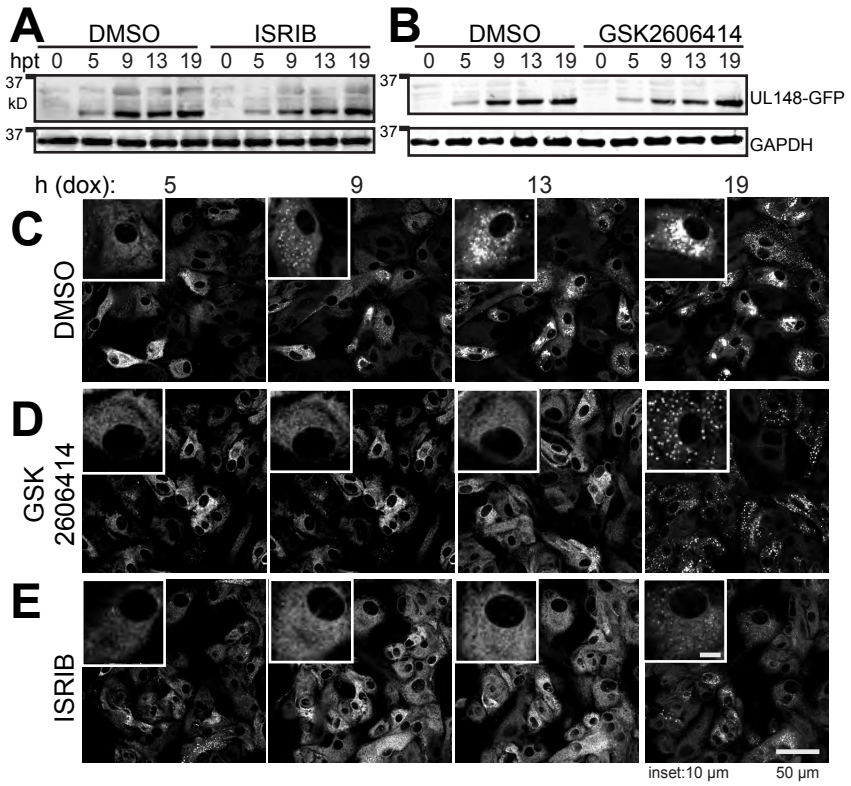

FIG 15. Inhibition of the integrated stress response impedes UL148-mediated ER remodeling. "Tet-on" ARPE-19 epithelial cells that inducibly express either UL148 or Rh159 fused to green florescent protein (gfp), i148^{gfp} (**A**) and i159^{gfp} (**B**), respectively, were induced for transgene expression using 100 ng/mL doxycycline (dox) in the presence of absence of either ISRIB (200 nM) or GSK2606414 (1.1 µM) and monitored by Western blot for expression of UL148-GFP over a series of time points (h post treatment with dox, hpt). (**C-E**): Live-cell imaging of UL148-GFP and Rh159-GFP expression patterns in the presence of ISRIB (200 nM), GSK2606414 (1.1 µM), or DMSO vehicle alone. Main scale bar represents 50 µm. For inset panels at upper left of each image, which are magnified 2.4× relative to the main image, the scale bar represents 10 µm. Also see SI Movies S8-S10.

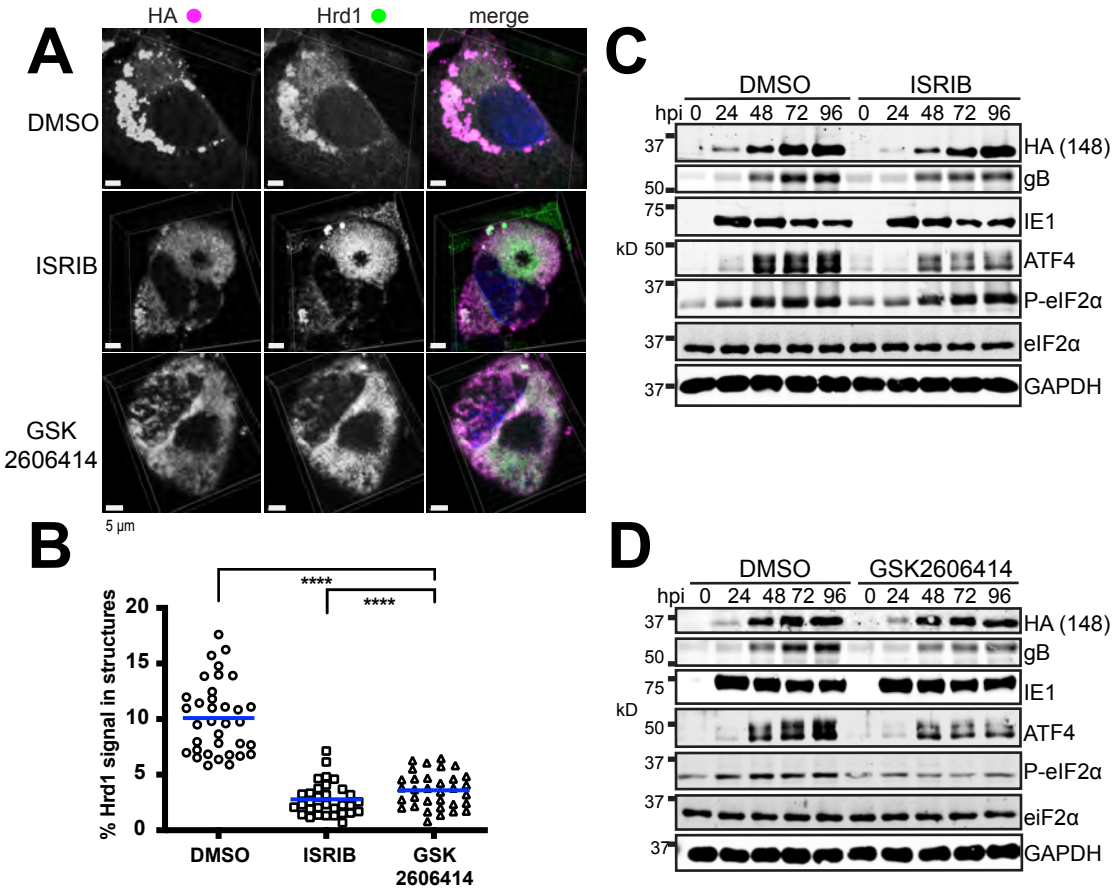

FIG 16. Inhibition of the ISR prevents the coalescence of Hrd1 and UL148 into discrete structures during infection. (**A**) Representative 3D maximum intensity projections of confocal imaging Z-stacks obtained from cells infected at MOI 1 for 96 h with HCMV strain TB40/E carrying an HA-tagged *UL148*, TB_148^{HA}, and maintained in the presence of ISRIB (200 nM), GSK2606414 (1.1 µM), or DMSO carrier alone (0.1% vol/vol). In merged images HA signal is shown in magenta, Hrd1 in green, and DAPI counterstaining in blue. (**B**) The percent of Hrd1 antibody signal involved in discrete structures at 96 hpi were calculated for a minimum of 30 cells per condition were determined using Imaris x64 9.3.0 software. Statistical significance was determined using a one-way ANOVA followed by Tukey's post-test; **** represents a P-value of <0.0001. The arithmetic mean for co-localization analysis results are shown as blue lines with data points for individual cells analyzed plotted as circles. (**C-D**) Western blot analyses of fibroblasts infected at MOI 1 with TB_148^{HA} and maintained in the presence of ISRIB (200 nM), GSK2606414 (1.1 µM), or DMSO carrier alone (0.1%); hpi: h post infection (hpi). Note: a phospho-specific antibody was used for detection of eIF2α phosphorylated at Ser51 (P-eIF2α).

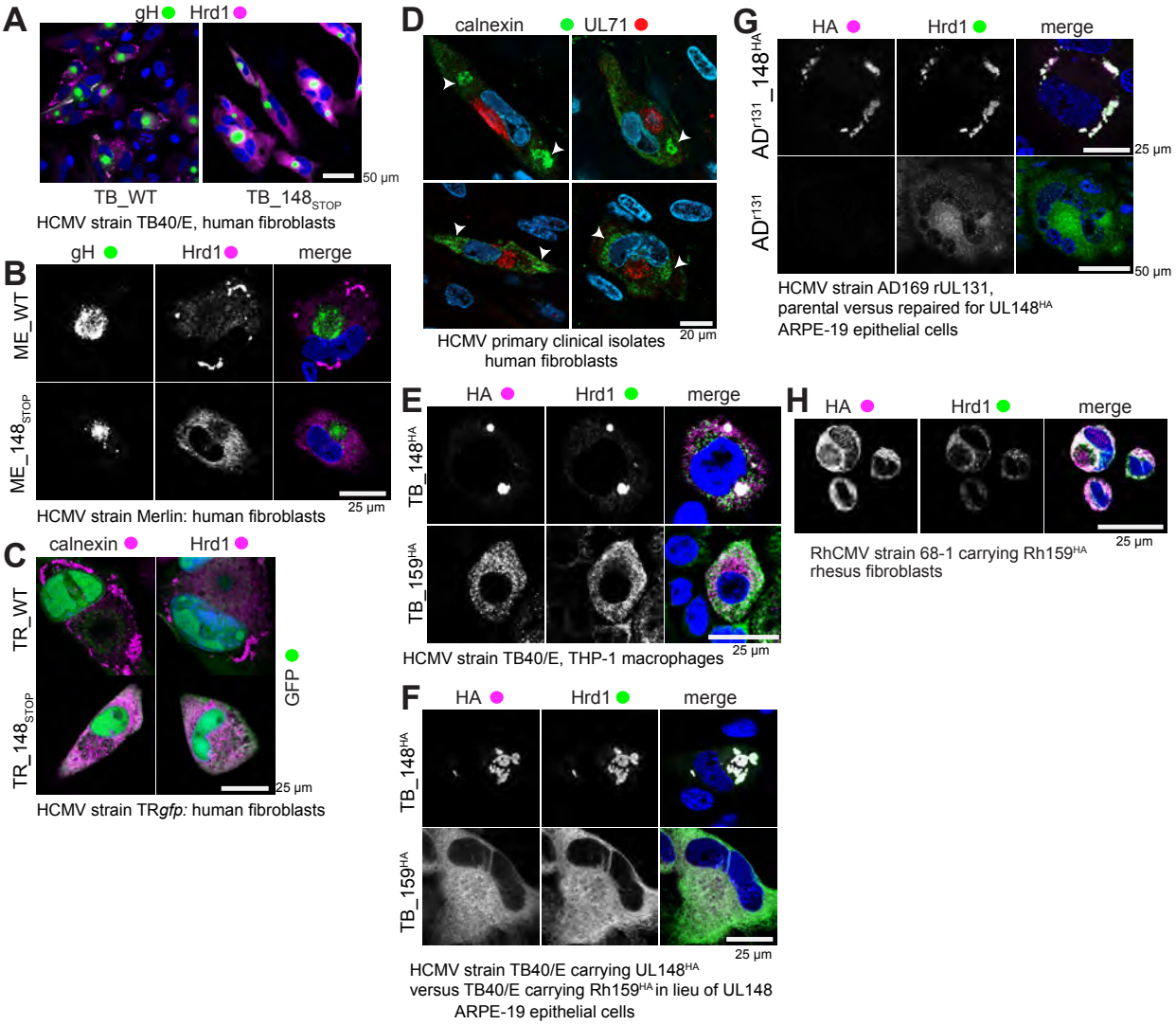

FIG S1: **Additional indirect immunofluorescent confocal microscopy results from infected cells.** (**A**) Lower magnification overview of results from FIGS 1A-B; staining of HCMV glycoprotein H (gH) and Hrd1 at 96 h postinfection (hpi) of human fibroblasts with wildtype HCMV strain TB40/E (WT) versus *UL148*-null derivative TB_148$_{STOP}$. (**B**) Staining of gH and Hrd1 at 96 hpi of human fibroblasts with wildtype Merlin recovered from BAC-cloned Merlin pAL1393 (ME_WT) or a *UL148*-null derivative of the same virus (ME_148$_{STOP}$.) (**C**): Staining of gH and Hrd1 at 96 hpi of human fibroblasts with wildtype HCMV strain TRgfp recovered from BAC-cloned TRgfp (TR_WT) or a *UL148*-null derivative of the same virus (TR_148$_{STOP}$). (**D**) Staining of the viral tegument protein UL71 and calnexin at 5 days postinfection of human fibroblasts with primary clinical HCMV isolates obtained from patient throat swabs. (**E**) Staining against HA and Hrd1 in THP-1 macrophages fixed at 96 hpi with HCMV strain TB40/E derivative viruses TB_148^{HA} or TB_159^{HA}; note: THP-1 monocytes were differentiated using phorbol ester treatment. (**F**) Staining of HA and Hrd1 in ARPE-19 epithelial cells infected for 96 h with either TB_148^{HA} or TB_159^{HA}. (**G**) Staining of HA and Hrd1 in ARPE-19 epithelial cells infected for 96 h with HCMV strain AD169 repaired for *UL131* and to which an HA-tagged UL148 CDS from TB40/E was restored to the native *UL148* locus (AD^{r131}_148^{HA}) or with a parental AD169 virus repaired for *UL131* to which *UL148* was not restored (AD^{r131}). Notes: (i) a functional *UL131* is required for efficient infection of epithelial cells; (ii) the difference in scale bar is because with ADr131 we did not employ a viral marker (e.g., HA) to identify infected cells, so the appearance of syncytia and the characteristic kidney-bean shaped nucleus was used to indicate infected cells and a slightly lower magnification was used to best show these features. (**H**) Staining for HA and Hrd1 in telomerase-immortalized rhesus fibroblasts infected with BAC-derived rhesus CMV (RhCMV) strain 68-1 carrying an HA-tag at the C-terminus of Rh159.

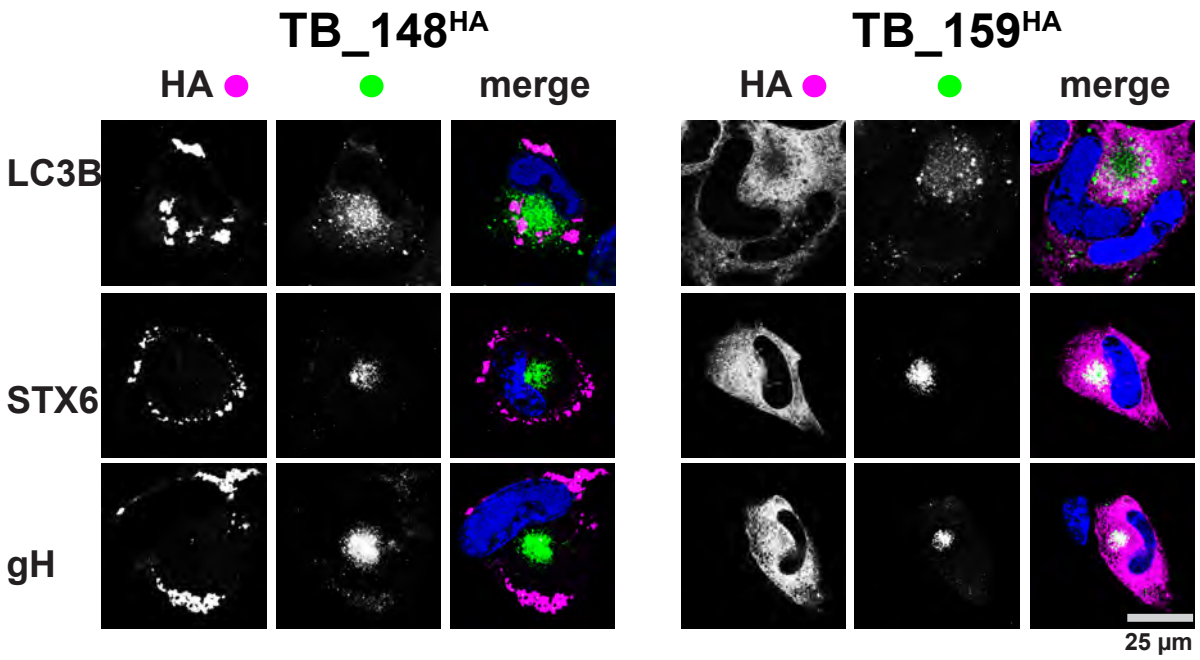

FIG S2: Confocal microscopy of LC3B, syntaxin-6 and glycoprotein H staining during HCMV infection. Human fibroblasts were infected with the indicated viruses for 96 h and then fixed, permeabilized, and stained using antibodies specific for the indicated proteins. Indirect immunofluorescence images were captured using a 63X objective on a Leica SP5 confocal microscope. gH: glycoprotein H, STX6: syntaxin-6.

TABLE S1. Oligonucleotide primers and synthetic DNAs used in this study

Name	Sequence (5' to 3')
148_eGFP_Fw	ACCTGGTGTCGCGGCGTCGGATGGTGAGCAAGGGGGAGGAGCTTTTTACTGGCGTTGTTC
Gibs_eGFP_Rv	CGGCCGCCACTGTGCTGGATTACTTATACAGCTCGTCCATACCCAG
Gib_148_Fw	TGTGGTGGAATTCTGCAGATTGCCACCATGTTGCGCTTGCTG
148_noStopRv	CCGACGCCGCGACACCAGGTAGGTTATC
159_eGFP_Fw	TCTAAAACGCAGTCGTGAAGCTCATATGGTGAGCAAGGGGGAGGA
159_noStop_Rv	ATGAGCTTCACGACTGCGTTTTAGAAGTG
Gibs_159_Fw	TGTGGTGGAATTCTGCAGATTGCCACCATGGCCTACAACAGC
Rh159_Fw	TGTGGTGGAATTCTGCAGATACCATGGCCTACAACAGCTTCCTTCTCAGCTGCCTTACCATCGCAC TTTTACTG
Rh159_HA_Rv	CGGCCGCCACTGTGCTGGATCTATTAGGCGTAGTCTGGGACGTCGTATGGGTAATGAGCTTCACG ACTGCGTTTTAGAAGTG
PpuISceKanGibs_Fw	CATTCACCTGAACCCATAGGTCCTGCCTGGCAGAGAATCTTAGGGATAACAGGGTAATCG
PpuISceKanGibs _Rv	AGATTCTCTGCCAGGCAGGACCTATGGGTTCAGGTGAATGGCCAGTGTTACAACCAATTA
Rh159_Fw_recomb	GGGCGGTGGCCGGCACGCCGCATTTCCTAACCCGCGCAGCATGGCCTACAACAGCTTCCT
Rh159_Rv_recomb	CGCGAACGACGTGTGACGAGGACGTGGTTTCCGCAAGCCTTTAGGCGTAGTCTGGGACG
TB_Rh159HA_seq_Fw	AGTGTTTATGAGTCGGGCGG
REV TB_Rh159HA_seq	GTGGCGACGTGGATTTCTTG
EGFP-P2A-3XHA	GTCGACTGGATCCGGTACCGAATTCGCCACCATGGTGAGCAAGGGGGAGGAGCTTTTTACTGGC GTTGTTCCCATCCTGGTTGAGTTGGATGGGGATGTCAACGGCCACAAGTTCAGCGTTTCTGGAGA AGGAGAAGGCGACGCAACCTATGGGAAGCTCACTTTGAAATTCATATGCACCACCGGTAAACTCC CAGTCCCCTGGCCTACCCTGGTCACTACCTTGACATATGGAGTTCAGTGCTTTTCTCGATACCCCG ACCACATGAAGCAGCACGATTTTTTCAAATCTGCAATGCCCGAGGGCTATGTACAAGAGAGGACCA TTTTCTTCAAAGACGACGGCAATTACAAGACCAGGGCCGAGGTCAAATTTGAAGGGGACACTCTTG TGAATCGGATCGAACTTAAAGGGATCGATTTCAAAGAGGACGGAAACATACTGGGGCATAAGCTG GAATACAACTACAATAGCCATAATGTTTACATTATGGCAGACAAGCAGAAAAACGGTATTAAGGTCA ACTTCAAGATACGGCATAACATTGAAGATGGGTCAGTCCAGCTTGCTGACCATTATCAGCAGAATA CACCCATTGGCGATGGTCCCGTGCTTTTGCCTGACAACCACTACCTTTCTACCCAAAGCGCATTGT CAAAAGATCCTAACGAGAAGAGAGATCATATGGTCCTTTTGGAGTTCGTAACCGCAGCTGGTATAA CTCTGGGTATGGACGAGCTGTATAAGGGCTCAGGGGCTACAAATTTTAGTCTCCTTAAACAAGCCG GAGATGTCGAAGAGAACCCTGGGCCTTACCCATATGACGTTCCTGACTATGCCGGTTACCCCTAT GATGTGCCAGATTATGCCGGATCTTATCCTTACGATGTACCTGACTATGCAGGTGGGAGTGGCAT GAATTACGTGGGGCAGC
Gibs_Age_159_Fw	CCGTACCACTTCCTACCCTCGTAAACCGGTGCCACCATGGCCTACAACAG
Gibs_Mlu_GFP_Rv	ACCCGGCGCGGAGGCCAGATCTTAACGCGTTTACTTATACAGCTCGTCCATACC
tRFP linker Fw	CCACTTCCTACCCTCGTAAACCGGTGAATTCGCCACCATGAGCGAGCTGAT
tRFP linker Rv	GCGCGGAGGCCAGATCTTAACGCGTGCGGCCGCTCGAGAATTCATCTGTGCCCCAGTTTGC

TABLE S2. Antibodies Used in Immunofluorescence Microscopy

Primary Antibody	Host species	Isotype	Clone	Vendor	Catalog No.	Dilution used
Calnexin	Mouse	mAb IgG1	37	BD Biosciences	610523	1:50
Calnexin	Rabbit	mAb IgG	C5C9	Cell Signaling Tech.	2679	1:50
Syntaxin 6	Rabbit	mAb IgG	C34B2	Cell Signaling Tech.	2869	1:50
SYVN1 (Hrd1)	Rabbit	mAb IgG	D3O2A	Cell Signaling Tech.	14773	1:500
SEL1L	Rabbit	pAb	n/a	Sigma	S3699	1:50
KDEL	Mouse	IgG2a	10C3	Enzo Life Sci., Inc.	ADI-SPA-827-D	1:50
PDI	Rabbit	mAb IgG	C81H6	Cell Signaling Tech.	3501	1:50
Herp (HerpUD1)	Rabbit	pAb IgG	n/a	Proteintech	10813-1-AP	1:50
VCP	Mouse	IgG2a	5	Invitrogen / Life Technologies	MA3-004	1:50
Calreticulin	Rabbit	mAb IgG	D3E6	Cell Signaling Tech.	12238	1:200
Ribophorin 1 (RPN1)	Rabbit	pAb IgG		ThermoFisher / Invitrogen	PA5-65662	1:50
EDEM-1	Mouse	mAb IgM	D-1	Santa Cruz	sc-377394	1;50
GABARAP	Rabbit	mAb	E1J4E	Cell Signaling Tech.	13733	1:200
LC3B	Rabbit	mAb	D11	Cell Signaling Tech.	3868	1:200
HA epitope	Chicken	IgY		Bethyl	A190-106A	1:200
HCMV glycoprotein H (gH)	Mouse	IgG2b	14-4b	Gift of William J. Britt, M.D.	n/a	1: 50
Reticulon-3 (RTN3)	Mouse	IgG2a		ThermoFisher / Invitrogen	MA5-15538	1: 200
HA epitope	Rabbit	pAb		Bethyl	A190-108A	1:1000
Secondary Antibody	**Host species**	**Isotype**		**Vendor**	**Catalog No.**	**Dilution used**
Alexa Fluor 488 anti-Mouse IgG (H+L), cross adsorbed	Goat	IgG		ThermoFisher / Invitrogen	A11001	1:1000
Alexa Fluor 488 anti-Rabbit IgG (H+L) Cross-Adsorbed	Goat	IgG		ThermoFisher / Invitrogen	A11008	1:1000
Alexa Fluor 594 anti-Rabbit IgG (H+L) Cross-Adsorbed	Goat	IgG		ThermoFisher / Invitrogen	A11012	1:1000
Alexa Fluor 594 anti-Mouse IgG (H+L) Cross-Adsorbed	Goat	IgG		ThermoFisher / Invitrogen	A11005	1:1000
Alexa Fluor 647 anti-Chicken IgY (H+L)	Goat	IgG		ThermoFisher / Invitrogen	A11039	1:1000